AD-A124 883 DIGITAL ESTIMATION AND CONTROL FOR AIR REFUELING RENDEZVOUS(U) AIR FORCE INST OF TECH WRIGHT-PATTERSON AFB OH SCHOOL OF ENGINEERING J T RIVARD DEC 82 1/1

UNCLASSIFIED AFIT/GA/EE/82D-1 F/G 12/1 NL

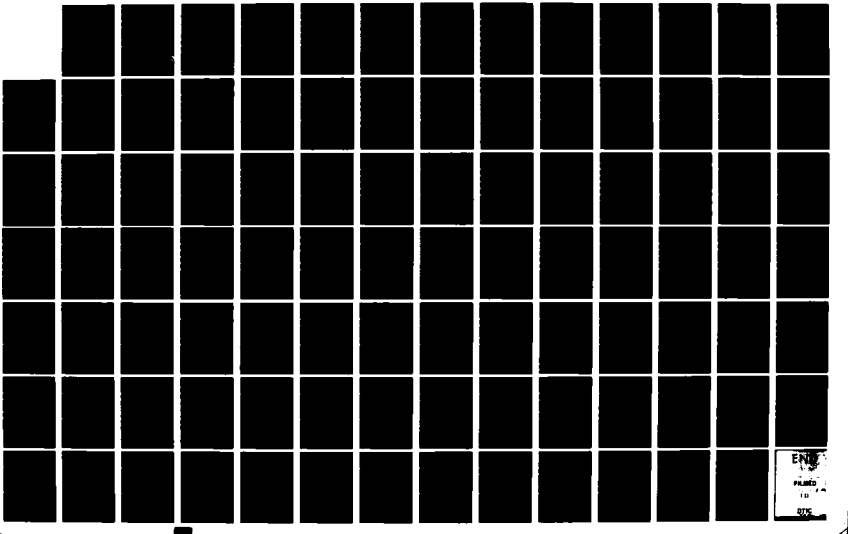

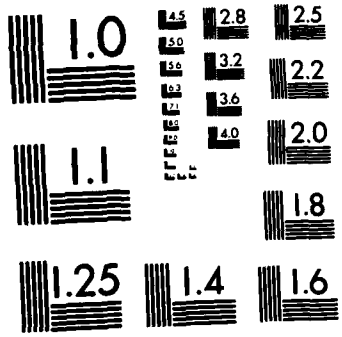

DIGITAL ESTIMATION AND CONTROL FOR AIR REFUELING RENDEZVOUS

THESIS

AFIT/GA/EE/82D-1 James T. Rivard
Capt USAF

DEPARTMENT OF THE AIR FORCE
AIR UNIVERSITY (ATC)
AIR FORCE INSTITUTE OF TECHNOLOGY

Wright-Patterson Air Force Base, Ohio

AFIT/GA/EE/82D-1

DIGITAL ESTIMATION AND CONTROL FOR AIR REFUELING RENDEZVOUS

THESIS

AFIT/GA/EE/82D-1 James T. Rivard
Capt USAF

AFIT/GA/EE/82D-1

DIGITAL ESTIMATION AND CONTROL FOR AIR REFUELING RENDEZVOUS

THESIS

Presented to the Faculty of the School of Engineering
of the Air Force Institute of Technology
Air University
in Partial Fulfillment of the
Requirements for the Degree of
Master of Science

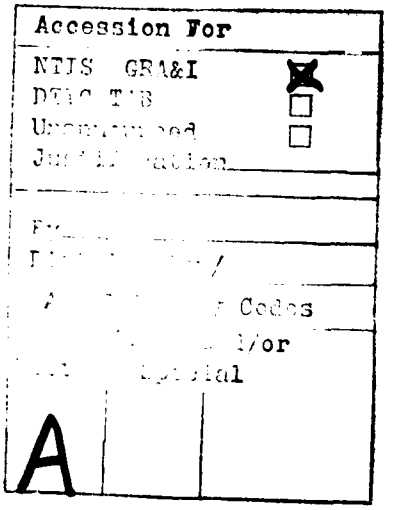

by
James T. Rivard, B.S.
Capt USAF
Graduate Astronautical Engineering
December 1982

Approved for public release; distribution unlimited

Preface

In 1980, the C-141B modification program began in earnest. Suddenly, C-141 flight crews had to develop expertise in an area in which they had virtually no experience - air refueling. The difficulties which many, including myself, encountered, prompted this research. Above all, this study's goal is simply to make things easier for the crewmember, who is given a variety of missions and limited training resources. Hopefully, this paper will cause others to look more closely at the air refueling problem in order to develop simpler, more efficient methods.

I am indebted to many people for their help in this effort. I am especially grateful to Lt Col Edwards for all of his advice, guidance, and patience. I would also like to thank all of those who assisted in the research, particularly Lt Ham and Greg Santaromita at Wright-Patterson, Maurice Johns with Delco, and Bob Harper at Collins. And, I am grateful that the typist, Linda Kankey, can meet a deadline better than I can.

James T. Rivard

Contents

Contents

List of Figures

List of Tables

Abstract

Estimation and control algorithms were developed for use by a tanker aircraft conducting an air refueling rendezvous. A stochostic model of a typical rendezvous was developed first. Then an entended Kalman filter which uses air-to-air TACAN distance measurements was designed. Also, algorithms were derived for computing the tanker's appropriate offset, turn point, and closed loop bank angle commands during the final turn of a point-parallel rendezvous.

In Monte Carlo simulations, a 3 state extended Kalman filter provided a stable, though limited, means of estimating the receiver's position and velocity throughout the rendezvous. Also, the control algorithms exhibited two advantages over the present rendezvous method: turn point solutions could be computed for other than nominal offsets and headings, and bank angle commands during the turn reduced position errors at rendezvous completion. When compared to the present method, root mean square, cross-track distance errors at rollout were reduced as much as 75%, and along-track errors were reduced up to 47%.

DIGITAL ESTIMATION AND CONTROL FOR AIR REFUELING RENDEZVOUS

I Introduction

Certainly, in-flight refueling is a vital element of Air Force strategy and tactics. It has long been a critical part of bomber and fighter operations. Recently it has assumed an increasingly important role in airlift planning as well, particularly with the advent of the Rapid Deployment Force. The Air Force's large fleet of KC-135 and KC-10 aircraft provide the United States with a unique military capability. No other nation in the world can project, in a matter of hours, such a wide range of military responses to a perceived threat anywhere in the world.

Of course the great advantage of in-flight refueling is that it eliminates the need for enroute airfields. Many navigational systems have been designed to get an aircraft safely into an airfield. However, there are no systems in operational use designed specifically for conducting air refueling rendezvous. Instead, a wide variety of navigation and radar systems designed primarily for other purposes are adapted to the problem. The two aircraft usually get together, but the initial rendezvous attempt is often very inaccurate. That frequently causes excessive maneuvering and delays in completing the join-up. Those undesirable effects take on additional significance for large aircraft requiring extended refueling time, aircraft formations, and refueling operations at night or in instrument weather conditions.

Hardware technology exists which should meet any practical rendezvous specification. The first step in upgrading our air refueling systems, though, is to investigate what improvements can be made with the existing equipment.

The KC-135 fleet was recently equipped with an inertial navigation system (INS). An integral part of the INS is the navigation computer. This computer uses information from the inertial instruments and the central air data computer (CADC) to compute aircraft position and velocity, and wind information. It also calculates steering commands for the autopilot and flight director system. The KC-135 and all Air Force refuelable aircraft are also equipped with Air-to-Air TACAN (Tactical Air Navigation). The system provides a measurement of straight line distance to other TACAN equipped aircraft.

A possible system improvement would be for the tanker to use TACAN measurements as inputs to an estimation algorithm which has outputs of the other aircraft's position and velocity. These estimates would then be used to compute steering commands for the tanker during the final part of the rendezvous. If all of those estimation and guidance computations can be handled by the present onboard navigation computer, the system could be implemented entirely on current hardware.

The purposes of this study are to develop an estimation and control method for solving the rendezvous problem and to see what improvements in accuracy such a system might achieve.

Along with the existing hardware constraint, operational feasibility is a prime consideration throughout. The standard rendezvous profile is altered as little as possible so that present methods can always be used as a back-up.

II Air Refueling Rendezvous

The most common type of rendezvous is called the point parallel rendezvous. In this type, the tanker waits for the receiver, the aircraft to be refueled, at a planned point along the receiver's route of flight. The rendezvous is accomplished and the refueling completed on a refueling track in the receiver's general direction of flight. This type of rendezvous will be discussed here.

Rendezvous Problem

A typical point parallel rendezvous is depicted in Figure 1. The tanker waits at refueling altitude in a holding pattern at the control point (CP). When the receiver reports that he has passed the initial point (IP), the tanker departs the holding pattern and flies towards the receiver. Meanwhile, the receiver proceeds along the refueling track at constant airspeed and descends to an altitude 1000 feet below the tanker. The tanker attempts to establish the correct offset and turn at the right time so as to roll out of a 30 degree bank turn two nautical miles directly in front of the receiver. The receiver then closes to one mile from which point the rendezvous is completed visually.

The rendezvous problems for the tanker, then, are to compute and fly the appropriate offset, turn at the correct time, and maintain proper bank angle throughout the turn.

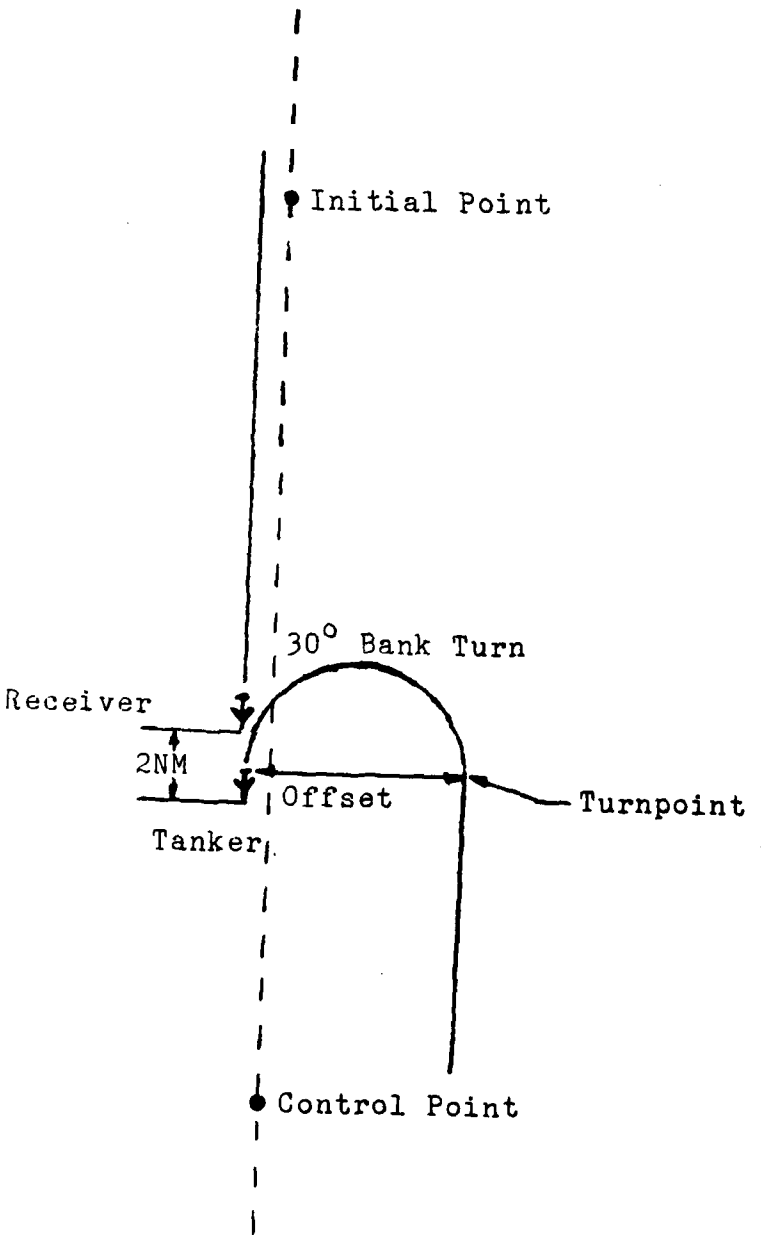

Figure 1. Point Parallel Rendezvous

Present Method

Currently, a chart is used to determine the correct offset and turn point. Given values for receiver true airspeed and drift angle, the chart gives the appropriate offset and distance from the receiver to initiate a 30 degree bank turn. Here, drift angle, the number of degrees the aircraft must crab into the wind to maintain a course parallel to the refueling track, is used as a measure of the wind component perpindicualr to the track. Since the tanker and receiver navigation systems do not agree exactly, they attempt to establish the desired offset by observing the other aircraft's position on radar. When the tanker's TACAN and/or radar indicates the receiver is at the calculated turn range, the tanker rolls into a 30 degree bank turn which he holds until he has turned to the refueling heading.

The present method has several inaccuracies. The offset and turn range chart only gives distances to the nearest mile; fluctuations in wind or airspeed are not compensated for; equipped with a radar designed primarily for weather, it is difficult for the KC-135 to determine accurately another aircraft's position; and, finally, the system is entirely open loop: a constant 30 degrees of bank is held throughout the turn. Even under the best visual conditions it is difficult for either the tanker or receiver to recognize any need for corrections until the turn is nearly complete.

Proposed Method

The proposed method would be basically the same procedure but with two improvements. Rather than using a chart, the correct offset and turn point would be calculated and periodically updated by the navigation computer. Also, an estimation algorithm using Air-to-Air TACAN distance measurements would be used to estimate continuously the receiver's position and velocity. That estimate would be used as input to a closed loop digital control algorithm before and during the turn.

A rendezvous conducted with such a system might proceed as follows:

1. Rendezvous data is loaded into tanker's INS anytime prior to rendezvous. Data includes control point coordinates, refueling track heading and altitude, and receiver altitude and airspeed.
2. Using these input data and information from the tanker's INS and central air data computer, the navigation computer calculates and displays the appropriate offset.
3. Tanker and receiver attempt to establish correct offset using radar.
4. Estimator is initialized based on planned receiver track, altitude, and airspeed, and computed wind velocity. A manual radar update might also be used.

5. Estimation algorithm propagates receiver state estimate and uses TACAN measurements for updates.
6. Computer calculates and displays time until turn and commands a turn at updated turn point.
7. Digital controller provides bank angle commands to the autopilot/flight director to reduce error at rollout.

The first step in designing such a system is to create a mathematical model of the rendezvous procedure just described. That model will later be used as the starting point for the estimator design, and as a reference or truth model for computer simulations.

III Truth Model

Research was conducted into present air refueling procedures, the KC-135 inertial navigation system, TACAN systems, and wind models. The result, as developed in this section, is a stochastic state differential equation and measurement equation which hopefully describe the actual dynamics, uncertainties, and errors reasonably well. For different types of receiver aircraft, the form of the state equations will be the same. However, there will be slight variations in certain parameters and error statistics due to different rendezvous airspeeds and navigation equipment. In the truth model development and the simulations, a standard rendezvous with a C-141 is modelled. This study, while limited to one aircraft type, should indicate both the practicality and the potential benefit of the proposed system.

Coordinate System

The coordinate system for the truth model is depicted in Figure 2. It is a simple, two-dimensional, rectangular system parallel to the tanker's local horizon plane. The origin is located at the control point (CP) at refueling altitude. The plus x axis points towards the initial point (IP), and the plus y axis is oriented as shown. Aircraft headings, Ψ, are measured counter-clockwise from the plus x axis.

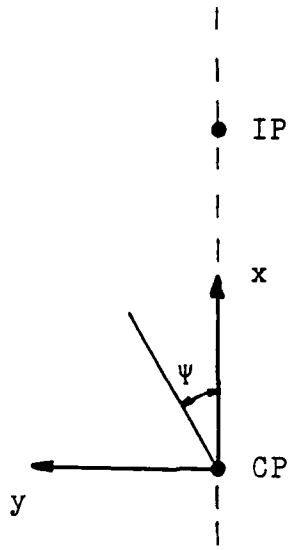

Figure 2. Coordinate System

The exact reference frame location and orientation are defined by the INS, so the frame varies slightly from a true ground fixed system due to INS errors. The advantage of defining the system by the INS is that INS tanker position readouts are deterministic rather than random variables.

Rectangular coordinates are chosen to make the filter state propagation equations linear. Also, this particular axes orientation simplifies turn point calculations: y position coordinates determine offset, and x position and velocity components determine the time to turn.

Receiver Dynamics

For an aircraft, the velocity in a ground fixed frame is found from

$$\underline{v} = \underline{v}_{a/w} + \underline{v}_{w} \tag{1}$$

where $\underline{v}$ is velocity relative to the ground, $\underline{v}_{a/w}$ is velocity of the aircraft relative to the wind or air mass, and $\underline{v}_w$ is the velocity of the wind.

The receiver attempts to fly a ground track along the x axis. In order to do so, he must apply a drift correction, δ, into the wind such that the y component of velocity, v_y, is zero. Since he is heading in the -x direction, his heading will then be $\Psi=\pi + \delta$.

The receiver pilot will also attempt to maintain a preplanned indicated airspeed. The tanker can convert this indicated airspeed to an equivalent true airspeed, v_R, based on rendezvous altitude and measured air temperature. The components of $\underline{v}_{a/w}$ are then

$$v_{a/w\ x} = v_R \cos(\pi + \delta)$$

and

$$v_{a/w\ y} = v_R \sin(\pi + \delta)$$

or, equivalently,

$$v_{a/w\ x} = -v_R \cos \delta$$

and

$$v_{a/w\ y} = -v_R \sin \delta$$

If the receiver maintains $v_y = 0$, the y component of Eq(1) becomes

$$0 = -v_R \sin \delta + v_{wy}$$

which can be used to find δ.

The navigation computer continuously calculates the wind vector, $\underline{v}_w$, by subtracting $\underline{v}_{a/w}$ - determined from measured true airspeed and aircraft heading - from the INS computed velocity, $\underline{v}$. The planned refueling track heading can then be used to calculate v_{wx} and v_{wy}.

Now the velocity relations for the receiver can be written. The receiver attempts to fly such that

$$\delta = \sin^{-1}\left[\frac{v_{wy}}{v_R}\right] \tag{2}$$

$$v_y = 0$$

and

$$v_x = -v_R \cos \delta + v_{wx} \tag{3}$$

Of course his flight will not exactly satisfy those equations. Instead, the actual velocity relations will be

$$v_y = v_{ye}$$

and

$$v_x = -v_R \cos \delta + v_{wx} + v_{xe}$$

where v_{xe} and v_{ye} are the velocity error components.

Cross-Track Error

As mentioned previously, the modelling parameters in this study are based on a standard rendezvous of a KC-135 and a C-141. Both aircraft are equipped with a Carousel IV inertial navigation system made by Delco. The C-141's autopilot can very

accurately maintain the course computed by its INS. The INS, though, drifts slightly during flight and is the source of some cross-track error.

Data from several hundred military and commercial flights indicated a 95% confidence figure of 1.65 NM/hr for the Carousel IV INS. According to Delco, a 95% cross-track confidence value can then be estimated as 66% x 1.65 NM/hr = 1.1 NM/hr (Ref 1: 6-1). Using this as a 2σ value, the INS has a 1σ cross-track error rate of 0.55 NM/hr.

Position errors in an INS have a variety of sources and the associated error models can be very elaborate (Ref 2). However, for the short time interval of a rendezvous - less than 10 minutes, the cross-track error might be reasonably modelled as the sum of a constant rate component and a small random walk component. Because the rendezvous duration is brief compared to the 84 minute Schuler period, and because this study is for feasibility and not detailed operational design, second-order, coupled error models are not included.

The random constant error rate, v_{yc}, models the long term position error source which flight tests have shown to be the dominant source of velocity error for the Carousel IV (Ref 1: 6-6). v_{yc} is assumed to be Gaussian and zero mean, and to have a standard deviation of 0.55 NM/hr. It is also assumed to be stationary: the error rate over a short period has the same statistics as the error rate over the whole flight. But that is only the error rate due to the receiver's INS. Remember that the receiver's

position and velocity are estimated in the reference frame of the tanker's INS. Any error in the tanker's INS is then perceived as an error in the receiver's state. So the total, apparent, constant drift rate is

$$v_{yc} = v_{yc\ \text{Receiver}} - v_{yc\ \text{Tanker}}$$

Since each INS operates independently, and the two aircraft may fly entirely different routes to the rendezvous, their random drift rates are assumed to be independent. Then v_{yc} is zero mean, Gaussian, and

$$\sigma^2_{vyc} = \sigma^2_{vyc\ \text{Receiver}} + \sigma^2_{vyc\ \text{Tanker}}$$

σ_{vyc} is thus calculated to be 0.778 NM/hr.

A random walk component of position error, y_w, is added to account for small deviations from the simplistic, constant error rate model. This component is modelled by

$$y_w(t) = w_y(t)$$

where $w_y(t)$ is a zero mean, continuous, white noise, and

$$E\{w_y(t)\ w_y\ (t+\tau)\} = q_y\delta(\tau)$$

$E\{\cdot\}$ is the expected value operator, $\delta(\cdot)$ is the Dirac delta function, and q_y is called the strength of the white noise. This type of model results in a zero mean process with

$$E\ \{y_w^2\ (t)\} = q_y(t-t_o)$$

where t_o is the initial time of the simulation.

Choosing an appropriate value for q_y was somewhat arbitrary. Schuler oscillations contribute a 0.2 NM/hr CEP velocity error component (Ref 1: 6-6). Over the short 10 minute rendezvous period, a 0.2 NM/hr error would cause a 202 ft position error. To account for both aircraft's errors, INS errors for which no error data could be found, and autopilot errors, a 1σ value for y_w at the end of a 10 minute period was chosen to be 500 ft. The idea here was to choose a conservative (high) value for the magnitude of the errors not modelled by v_{yc}. Since the proposed method would have to be suitable for several receiver aircraft types, a specific C-141 INS error model is inappropriate. The noise strength is then found to be

$$q_y = \frac{(500 \text{ ft})^2}{(10 \text{ min})} = 25000 \text{ ft}^2/\text{min}$$

$$= 1.13 \times 10^{-5} \text{ NM}^2/\text{sec}$$

The model for cross-track position and velocity is now written as

$$\dot{y}(t) = v_{ye}(t)$$

$$v_{ye}(t) = v_{yc} + w_y(t)$$

$$E\{v_{yc}\} = 0, \ \sigma_{vyc} = 2.161 \times 10^{-4} \text{ NM/sec}$$

$$E\{w_y(t)\} = 0, \ q_y = 1.13 \times 10^{-5} \text{ NM}^2/\text{sec}$$

Now, only the initial condition statistics for y(t) remain to be specified. In the simulations, two different situations are modelled. In one case, the rendezvous is conducted without the assistance of radar and each aircraft is navigating solely off of its unaided INS. Assuming the two aircraft's INS errors are independent, Gaussian, zero mean, and have a 1σ error rate of 0.55 NM/hr, y(0) is also zero mean, Gaussian with

$$\sigma_{yo}^2 = (0.55\ t_{aR})^2 + (0.55\ t_{aT})^2$$

Here t_{aR} and t_{aT} are the airborne times, in hours, of the receiver and tanker. For an airborne time of 10 hours for the C-141 and 5 hours for the KC-135, σ_{yo} is computed to by 6.15 NM. Of course this much total error would be extreme. Normally, one or both aircraft would have the opportunity to update its INS somewhere enroute, or the rendezvous track may be defined by radio navigation aids. This "worst case" is included to get a feel for the limitations, if any, of the proposed system.

The case in which radar is used to help estimate the receiver's position is also modelled. In this case

$$E\{y(0)\} = y_T(0) + \Delta\hat{y}_o$$

where y_T is the tanker's y coordinate and $\Delta\hat{y}_o$ is a manually inserted estimate of the lateral distance between the two aircraft. The accuracy of this estimate varies with range. Error due to radar azimuth misalignment decreases linearly with range. Also, at shorter ranges the radar display can be set to

a smaller scale. No data on the accuracy of such an estimate could be found, so a σ_{yo} value was assumed. From personal experience, it seemed reasonable to say that a crewmember can estimate bearing from a radar display to a 1σ accuracy of 2 degrees. At 60 NM range, a 1 degree azimuth error results in about a 1 NM cross-track error. The relationship between azimuth and cross-track error is nearly linear, so a 1σ azimuth error is assumed to cause a σ_{yo} value of 2 NM for a 60 NM radar range, and a σ_{yo} value of 1 NM for a 30 NM radar range.

Along-Track Error

The receiver's along-track position and velocity components are modelled by

$$\dot{x} = v_x$$

$$v_x = -v_R \cos \delta + v_{wx} + v_{xe} \qquad (4)$$

The tanker can convert the receiver's planned indicated airspeed to the true rendezvous airspeed, v_R, using altitude and air temperature data from its central air data computer (CADC). INS and CADC data can also be combined to compute the wind velocity components, v_{wx} and v_{wy}. Using Eq(2), δ is then calculated. These estimated values for v_R, δ, and v_{wx} are only computed at the start of the rendezvous and remain constant. In Eq(4), v_{xe} is then treated as the only random variable. v_R, δ, and v_{wx} could be continuously updated, but then the spatial correlation of those computed values and v_{xe} would have to be accounted for

in the truth and filter models. Certainly this would be an area for future consideration, but it was considered beyond the scope of this study.

v_{xe} is modelled as the sum of a random constant and an exponentially-correlated component. The constant component is primarily due to instrumentation and pilot bias errors. This bias would include factors such as tanker errors in computing the wind components, error in the receiver's displayed airspeed, the receiver pilot's inability to maintain the correct airspeed on average, and differences in temperature between the two aircrafts' positions when v_R is computed. To get a rough idea of the magnitude of this bias error, the individual error sources were assigned variances. The figures used were not explicitly listed as standard deviations; approximate 1σ values had to be surmised from published CEP values and tolerances, computer flight plans, and personal experience. The following 1σ error values were used: tanker ground speed - 1 knot (Ref 1: 6-6), tanker and receiver true airspeed - 2 knots each (Ref 1: 7-5), airspeed change due to change in temperature between IP and CP - 1 knot (Ref 3: 10-17, 30), and pilot error - 5 knots.

Since the total error is the sum of each of these components, and they are each assumed to be independent, the variance of the total error is the sum of the individual variances. The result is a variance of $35 NM^2/hr^2$. The random constant component of error, v_{xc}, is then modelled as Gaussian, zero mean, with a standard deviation of 6 NM/hr.

The correlated component is due mainly to wind fluctuations. Wind data is difficult to interpret. The models can be very complicated and vary considerably with the altitude and frequency ranges considered. A basic approximation, though, is that wind velocity is exponentially, spatially correlated (Ref 4: 2). Aircraft ground speed is mainly affected by just the slowly varying winds since high frequency gusts have no net effect on aircraft displacement. An exponentially correlated wind model, with a correlation distance of 50 NM, was adopted from (Ref 4: 2).

In the time domain, v_{xf}, the fluctuating component of along-track velocity error, is modelled by the equation

$$\dot{v}_{xf}(t) = -\frac{1}{T_f} v_{xf}(t) + w_f(t)$$

where T_f is the time constant, and $w_f(t)$ is a continuous white noise process. T_f is found from the equation

$$T = \frac{\text{Correlation distance}}{\text{Airspeed}}$$

to be 455 sec for a C-141 traveling at 396 knots. A 1σ value of 10 knots was chosen for $v_{xf}(t)$. This figure seemed reasonable after examining forecast wind variations along refueling tracks on actual computer generated flight plans (Ref 3: 10-17, 30). The appropriate strength of the zero mean, white, Gaussian noise $w_f(t)$ is found from the equation

$$q = \frac{2\sigma^2}{T} \qquad \text{(Ref 5: 178)} \qquad (5)$$

to be $3.39 \times 10^{-8} NM^2/sec^3$. The resulting $v_{xf}(t)$ process is zero mean, as it should be if the wind velocity at the tanker's position is considered the mean wind. Remember that v_{xf} is not the total wind, it is just the fluctuating component of deviation from an estimated wind, v_{wx}.

Altitude Separation

In the truth model, position and velocity components are measured in the local-level coordinate frame discussed earlier. However, the receiver will actually be displaced vertically from the reference plane due to a planned altitude separation, altimeter errors, and the curvature of the earth.

The planned altitude separation, a_o, is usually 1000 ft or 0.164 NM. Altimeter error, though, will cause some deviation from a_o, even if both aircraft are using the same altimeter setting. When flying at a constant altitude over a relatively short distance, the error is essentially constant (Ref 6: 4-4). A zero mean, Gaussian random bias is then used to model the net error. Maximum acceptable error before takeoff is 75 feet, but the error increases slightly with altitude. For the simulated rendezvous altitude of 25000 ft, a standard deviation of 150 ft or 0.0247 NM is assumed (Ref 7: 1-5, 1-6).

The further away the receiver is from the tanker, the more it will fall below the tanker's local-horizon reference plane. The amount of vertical displacement is $r_e(1 - \cos \phi)$ where r_e is the radius of the earth, and ϕ is the angle of

central arc which separates the two aircraft. The angle ϕ can be found from

$$\phi = \frac{s}{r_e}$$

where s is the arc length between the two aircraft. For the short distances involved - less than 100 NM, s is approximated by d, the straight line distance between the tanker and receiver. A value of 3444 NM is used in the simulations for r_e.

The altitude separation model is then

$$a = a_o + a_e + a_c$$

where a is the total altitude separation, a_o is the planned separation, a_e is altimeter error, and a_c is vertical displacement due to the curvature of the earth.

Incidentally, the velocity component v_x, as viewed from the tanker, will also be affected slightly due to the curvature of the earth. The receiver's velocity vector is oriented out of the horizontal plane by the angle ϕ described above. However, the maximum horizontal velocity change due to this effect is less than 0.2 NM/hr for a receiver true airspeed of 400 NM/hr. At the initial TACAN ranges, where this effect is the greatest, the final estimator design only achieved a 1σ accuracy of about 10 NM/hr, so ignoring this effect in the truth model does not affect the simulation results.

TACAN Error

With air-to-air TACAN, the tanker can measure the straight-line distance to another TACAN equipped aircraft. TACANs can also provide a bearing measurement to TACAN ground stations, but the KC-135's current system does not provide bearing capability for air-to-air operation (Ref 10: 1). The TACAN error model used in (Ref 4: 3) and (Ref 8: 18) was adopted. TACAN measurements are modelled by the equations

$$d_T(t) = d(t) + d_e(t)$$

and

$$d_e(t) = b + n(t)$$

where d_T is the TACAN measured distance, d the true distance, and d_e the TACAN error. The error is the sum of a random bias, b, and a short correlation time component, n.

The KC-135 was recently equipped with an improved system, the AN/ARN 118 (V) TACAN made by Collins. Test results (Ref 9: 1), published tolerances (Ref 10: 9), and flight test results of a similar system (Ref 11: 16) indicate the model described above is reasonable, but that the standard deviations for b and n are less than those used previously.

The bias, b, is modelled as zero mean, normally distributed (Ref : 3), and having a standard deviation of 0.1 NM (Ref 10: 9). n(t) is modelled as a zero mean, Gauss-Markov process (Ref 4: 3) generated by the system

$$\dot{n}(t) = -\frac{1}{T_n} n(t) + w_n(t)$$

The correlation time, T_n, is 3.6 sec (Ref 4: 3). The standard deviation of n, for the new TACAN, is 0.016 NM (Ref 9: 1) (Ref 11: 16). The appropriate strength of the continuous, white Gaussian noise process is found from Eq(5) to be $1.422 \times 10^{-4} NM^2/sec$.

Summary

The entire truth model is summarized below. Random variables are underscored with a tilde, and mean and standard deviation values are denoted by m and σ respectively. Non-random variables, such as v_R, are determined from planned rendezvous parameters, and INS and CADC data. The listed values are those used in the simulations.

$$\delta = \sin^{-1}\left[\frac{v_{wy}}{v_R}\right] \tag{6}$$

δ = Drift correction

v_{wy} = y component of wind

v_R = Receiver true airspeed

$v_R = 0.110$ NM/sec (396 NM/hr)

$$\dot{\underset{\sim}{y}}(t) = \underset{\sim}{v}_{yc} + \underset{\sim}{w}_y(t) \tag{7}$$

$\underset{\sim}{y}(t)$ = Receiver's y coordinate

No radar aiding:

$m_{yo} = 0$, $\sigma_{yo} = 6.15$ NM

With radar aiding:

$$m_{yo} = y_T(0) + \Delta\hat{y}_o$$

where y_T = Tanker y coordinate

$\Delta\hat{y}_o$ = Estimated offset

σ_{yo} = 1 NM for 30 NM radar range

$\underset{\sim}{v}_{yc}$ = Constant component of lateral drift

$m_{vyc} = 0$, $\sigma_{vyc} = 2.161 \times 10^{-4}$ NM/sec (0.778 NM/hr)

$\underset{\sim}{w}_y(t)$ = Continuous white noise

$m_{wy} = 0$, $q_y = 1.13 \times 10^{-5}$ NM^2/sec

$$\dot{\underset{\sim}{x}}(t) = -v_R \cos\delta + v_{wx} + \underset{\sim}{v}_{xc} + \underset{\sim}{v}_{xf}(t) \qquad (8)$$

$\underset{\sim}{x}(t)$ = Receiver x coordinate

v_{wx} = x component of wind

$\underset{\sim}{v}_{xc}$ = Constant component of x velocity deviation

$m_{vxc} = 0$, $\sigma_{vxc} = 2.78 \times 10^{-3}$ NM/sec (10 NM/hr)

$\underset{\sim}{v}_{xf}$ = Fluctuating component of deviation

$m_{vxf} = 0$, $\sigma_{vxf} = 1.67 \times 10^{-3}$ NM/sec (6 NM/hr)

$$\dot{\underset{\sim}{v}}_{xf}(t) = -\frac{1}{T_f}\,\underset{\sim}{v}_{xf}(t) + \underset{\sim}{w}_f(t) \qquad (9)$$

T_f = Correlation time

T_f = 455 sec

$\underset{\sim}{w}_f(t)$ = Continuous white noise

$$m_{wf} = 0, \; q_f = 3.39 \times 10^{-8} NM^2/sec^3$$

$$\underset{\sim}{a} = a_o + \underset{\sim}{a}_e + a_c \tag{10}$$

$\underset{\sim}{a}$ = Altitude separation

a_o = Planned separation

$$a_o = 0.164 \text{ NM (1000 ft)}$$

$\underset{\sim}{a}_e$ = Altitude error

$$m_{ae} = 0, \; \sigma_{ae} = 0.0274 \text{ NM (150 ft)}$$

a_c = Separation due to curvature of the earth

$$a_c = r_e \{1-\cos(d/r_e)\}$$

r_e = 3444 NM

d = Distance between aircraft

$$\underset{\sim}{d}_e(t) = \underset{\sim}{b} + \underset{\sim}{n}(t) \tag{11}$$

$\underset{\sim}{d}_e(t)$ = TACAN measurement error

$\underset{\sim}{b}$ = TACAN bias

$$m_b = 0, \; \sigma_b = 0.1 \text{ NM}$$

$\underset{\sim}{n}(t)$ = Short correlation component of error

$$m_n = 0, \; \sigma_n = 0.0160 \text{ NM}$$

$$\dot{\underset{\sim}{n}}(t) = -\frac{1}{T_n}\underset{\sim}{n}(t) + \underset{\sim}{w}_n(t) \tag{12}$$

T_n = Correlation time

$T_n = 3.6$ sec

$\underset{\sim}{w}_n(t)$ = Continuous white noise

$m_{wn} = 0,\ q_n = 1.422 \times 10^{-4} NM^2/sec$

In matrix form, the dynamics are described by

$$\frac{d}{dt}\begin{bmatrix} x \\ v_{xc} \\ v_{xf} \\ y \\ v_{yc} \\ a_e \\ b \\ n \end{bmatrix} = \begin{bmatrix} 0 & 1 & 1 & 0 & 0 & 0 & 0 \\ 0 & 0 & 0 & 0 & 0 & 0 & 0 \\ 0 & 0 & -1/T_f & 0 & 0 & 0 & 0 \\ 0 & 0 & 0 & 0 & 1 & 0 & 0 \\ 0 & 0 & 0 & 0 & 0 & 0 & 0 \\ 0 & 0 & 0 & 0 & 0 & 0 & 0 \\ 0 & 0 & 0 & 0 & 0 & 0 & 0 \\ 0 & 0 & 0 & 0 & 0 & 0 & -1/T_n \end{bmatrix} \begin{bmatrix} x \\ v_{xc} \\ v_{xf} \\ y \\ v_{yc} \\ a_e \\ b \\ n \end{bmatrix} + \begin{bmatrix} -v_R \cos\delta + v_{wx} \\ 0 \\ 0 \\ 0 \\ 0 \\ 0 \\ 0 \\ 0 \end{bmatrix}$$

$$+ \begin{bmatrix} 0 & 0 & 0 \\ 0 & 0 & 0 \\ 1 & 0 & 0 \\ 0 & 1 & 0 \\ 0 & 0 & 0 \\ 0 & 0 & 0 \\ 0 & 0 & 0 \\ 0 & 0 & 1 \end{bmatrix} \begin{bmatrix} w_f \\ w_y \\ w_n \end{bmatrix} \qquad (13)$$

As stated earlier, the linear form of this resulting dynamic equation motivated the specific choice of coordinate system.

The discrete measurements at time t_i are described by

$$\underset{\sim}{d}_T(t_i) = \sqrt{\{\underset{\sim}{x}(t_i) - x_T(t_i)\}^2 + \{\underset{\sim}{y}(t_i) - y_t(t_i)\}^2 + \{a_o + \underset{\sim}{a}_e + a_c\}^2} + \underset{\sim}{b} + \underset{\sim}{n}(t_i) \qquad (14)$$

With the truth model for state dynamics and measurements defined, attention will now be turned to designing an estimator to give the necessary navigational inputs to the rendezvous control algorithm.

IV Estimation

The design goal is a system which would enable the tanker to rendezvous more accurately with the receiver. The better the tanker estimates the receiver's position and velocity, the better he can determine where and when to turn. Also, a continuously updated estimate of the receiver's state would enable the tanker to use closed loop control during the final turn - a capability which does not exist with the present method. To provide such an estimate, a reduced order, extended Kalman filter was designed.

Extended Kalman Filter

The descrete, linear Kalman filter (Ref 5: Ch 5) is a commonly used estimation method. Its estimate of a state vector $\underline{x}$ is based on an assumed, linear, stochastic dynamics model of the form

$$\dot{\underline{x}}(t) = \underline{F}(t)\underline{x}(t) + \underline{B}(t)\underline{u}(t) + \underline{G}(t)\underline{w}(t) \tag{15}$$

where $\underline{u}(t)$ is a deterministic forcing function and $\underline{w}(t)$ is a continuous white noise, and a linear measurement equation

$$\underline{z}(t_i) = \underline{H}(t_i)\ \underline{x}(t_i) + \underline{v}(t_i) \tag{16}$$

where $\underline{z}(t_i)$ is a discrete measurement vector, and $\underline{v}(t_i)$ is a discrete white noise. The Kalman filter also assumes $\underline{x}(t_o)$, $\underline{w}(t)$, and $\underline{v}(t_i)$ to be Gaussian and mutually independent.

The dynamic and measurement equations developed for the truth model, Eqs(13) and (14), fit the standard Kalman filter form and assumptions except the measurement equation is nonlinear.

The extended Kalman filter is one means of handling such nonlinearities (Ref 12: Sec 9.5). It was chosen over higher order nonlinear filters (Ref 12: Ch 12) for this initial study because it is more likely to be operationally employed since it poses less computational burden.

In the extended Kalman filter, the nonlinear dynamic and measurement equations are linearized about the most recent state estimate. The result is a linear, state and measurement perturbation model. Now the standard Kalman filter update equations can be used to estimate the perturbation state $\delta \underline{x}$, and the state vector $\underline{x}$ can be updated by

$$\hat{\underline{x}}(t_i^+) = \hat{\underline{x}}(t_i^-) + \delta\underline{x}(t_i^+)$$

where the hat notation indicates an estimate, and the time arguments t_i^- and t_i^+ distinguish between state estimates before and after update.

For a problem such as this one, in which only the measurement equation is nonlinear, the extended Kalman filter can be summarized as follows:

Dynamics Model:

$$\dot{\underline{x}}(t) = \underline{F}(t)\underline{x}(t) + \underline{B}(t)\underline{u}(t) + \underline{G}(t)\underline{w}(t) \tag{17}$$

Measurement Model:

$$\underline{z}(t_i) = \underline{h}\{\underline{x}(t_i), t_i\} + \underline{v}(t_i) \tag{18}$$

Statistical Description of Uncertainties:

$$E\{\underline{x}(t_o)\} = \hat{\underline{x}}_o \qquad E\{(\underline{x}(t_o)-\hat{\underline{x}}_o)(\underline{x}(t_o)-\hat{\underline{x}}_o)^T\} = \underline{P}_o$$

$$E\{\underline{w}(t)\} = \underline{0} \qquad E\{\underline{w}(t)\underline{w}^T(t+\tau)\} = \underline{Q}(t)\,\delta(\tau)$$

$$E\{\underline{v}(t_i)\} = \underline{0} \qquad E\{\underline{v}(t_i)\underline{v}^T(t_i)\} = \underline{R}(t_i)\,\delta_{ij}$$

$$E\{\underline{v}(t_i)\underline{w}^T(t)\} = \underline{0}$$

where δ_{ij} is the Kronecker delta function.

State Propagation Between Updates:

$$\hat{\underline{x}}(t_i^-) = \underline{\Phi}(t_i,t_{i-1})\,\hat{\underline{x}}(t_{i-1}^+) + \int_{t_{i-1}}^{t_i} \underline{\Phi}(t_i,\tau)\underline{B}(\tau)\underline{u}(\tau)\,d\tau \tag{19}$$

$$\underline{P}(t_i^-) = \underline{\Phi}(t_i,t_{i-1})\underline{P}(t_{i-1}^+)\,\underline{\Phi}^T(t_i,t_{i-1}) + \int_{t_{i-1}}^{t} \underline{\Phi}(t_i,\tau)\underline{G}(\tau)\underline{Q}(\tau)\underline{G}^T(\tau)\underline{\Phi}^T(t_i,\tau)\,d\tau \tag{20}$$

where $\underline{\Phi}$ is the state transition matrix defined by

$$\frac{d}{dt}\underline{\Phi}(t,t_o) = \underline{F}(t)\,\underline{\Phi}(t,t_o),\ \underline{\Phi}(t_o,t_o) = \underline{I}$$

Measurement Update:

$$\underline{K}(t_i) = \{\underline{P}(t_i^-)\underline{H}^T(t_i)\,\underline{H}(t_i)\underline{P}(t_i^-)\underline{H}^T(t_i) + \underline{R}(t_i)\}^{-1} \tag{21}$$

where

$$\underline{H}(t_i) = \left.\frac{\partial\,\underline{h}\,(\underline{x},\,t_i)}{\partial\,\underline{x}}\right|_{\underline{x}\,=\,\hat{\underline{x}}(t_i^-)} \tag{22}$$

$$\delta\hat{\underline{x}}(t_i^+) = \underline{K}(t_i)\{\ \underline{z}(t_i) - \underline{h}\ (\hat{\underline{x}}(t_i^-),\ t_i)\ \} \tag{23}$$

$$\hat{\underline{x}}(t_i^+) = \hat{\underline{x}}(t_i^-) + \delta\hat{\underline{x}}(t_i^+) \tag{24}$$

$$\underline{P}(t_i^+) = \underline{P}(t_i^-) - \underline{K}(t_i)\underline{H}(t_i)\underline{P}(t_i^-) \tag{25}$$

Dynamics Model

The truth model equations, (13) and (14), could be used for the filter model as well. Then filter design would simply be a straightforward application of equations (17) through (25). However, unnecessary states mean unnecessary computations, and a trade-off should be made of computer loading versus filter performance. An analysis of the error states in the truth model indicates that the filter can probably be reduced to just three states without a significant loss of accuracy.

First of all, the altitude model can be simplified. The amount of altitude separation due to the curvature of the earth can be large, but it has little effect when estimating velocity or position in a horizontal plane. For example, for a distance between aircraft of 100 NM, a_c equals 1.45 NM. However, ignoring a_c would only cause a velocity estimate error of 0.17 knots and a position estimate error of 65 ft; at a closer range of 30 NM, the errors would only be 0.01 knots and 1.73 ft. A similar analysis of the effect of altimeter error shows that it, too, can be ignored. Even at the nominal rendezvous completion range of 2 NM, a 3σ altimeter error of 450 ft would only change

the horizontal position estimate by 45 ft. So, only the planned altitude separation term, a_o, is retained in the filter model.

The filter model was further simplified by dropping the measurement noise components from the state vector. The correlated component, n, with a 1σ value of 0.016 NM, is small compared to the bias, b, which has a 1σ value of 0.1 NM. Also, its short correlation time makes it appear to the filter as a discrete, uncorrelated noise. For example, with a sampling time interval of 10 seconds, the covariance of 2 consecutive samples of n is only $1.59 \times 10^{-5} NM^2$. It would seem advantageous to be able to estimate the bias. This was attempted; but as will be discussed further in Section VI, simulations indicated that b is relatively unobservable. When it is retained as part of the state vector, its variance decreases very little and no noticeable improvement in filter performance is attained. Therefore, in the final filter design, no attempt is made to estimate explicitly b or n.

In the truth model, the along-track states are modelled by

$$\dot{x}(t) = -v_R \cos\delta + v_{wx} + v_{xc} + v_{xf}(t) \tag{8}$$

But it would be difficult for an estimator to differentiate between the random constant v_{xc} and the slowly varying v_{xf}. One technique is to replace a bias plus long correlation time error with a random walk model (Ref 13: 2-3). $v_{xc} + v_{xf}$ is therefore replaced by a single state, v_{xe}, which is modelled by

$$\dot{v}_{xe}(t) = w_x(t)$$

where w_x is a continuous white noise.

Finally, the cross-track model is simplified. The truth model equation is

$$\dot{y}(t) = v_{yc} + w_y(t) \tag{7}$$

However, the magnitude of the random constant v_{yc} is so small that no attempt is made to estimate it explicitly. Instead, it is dropped from the filter state vector and the strength of the white noise is increased.

What is left is a simple, three state dynamics equation which only models the dominant states:

$$\begin{bmatrix} \dot{x} \\ \dot{v}_{xe} \\ \dot{y} \end{bmatrix} = \begin{bmatrix} 0 & 1 & 0 \\ 0 & 0 & 0 \\ 0 & 0 & 0 \end{bmatrix} \begin{bmatrix} x \\ v_{xe} \\ y \end{bmatrix} + \begin{bmatrix} 1 \\ 0 \\ 0 \end{bmatrix} (-v_R \cos + v_{wx}) +$$

$$\dot{\underline{x}} = \underline{F} \underline{x} + \underline{B} u +$$

$$\begin{bmatrix} 0 & 0 \\ 1 & 0 \\ 0 & 1 \end{bmatrix} \begin{bmatrix} w_x \\ w_y \end{bmatrix} \tag{26}$$

$$\underline{G} \quad \underline{w}$$

These states are also the only input data required by the controller.

In the reduced order filter model, there is no exact way of setting the noise strengths. Experimentation, or tuning, will determine which values are chosen. Some reasoning can be used, though, to arrive at initial trial values for $\underline{Q}$.

When replacing one model with another simpler one, it would seem appropriate for the outputs of both models to be changing value in some similar manner. For an exponentially correlated component replaced by a random walk, an empirically found, useful technique is to set

$$q = \frac{\sigma^2}{\tau}$$

where σ^2 is the correlated process variance and τ is the correlation time (Ref 13: 2-3). This method was used to find an appropriate strength for w_x:

$$q_x = \frac{\sigma^2_{vxf}}{T_f} = 1.69 \times 10^{-8} NM^2/sec^3$$

A similar insight was used to set q_y. The one sigma cross-track position error was said earlier to be $0.55t_a$ NM where t_a is the time in hours since alignment. The net cross-track error at rendezvous, then, has a variance of

$$\sigma^2_y(t) = (0.55t_{aT})^2 + (0.55t_{aR})^2 = 0.3025(t_{aT}^2 + t_{aR}^2)$$

where t_{aT} and t_{aR} are the airborne times of the tanker and receiver at rendezvous. By taking the derivative of $\sigma^2_y(t)$ with respect to time, it is found that the variance at rendezvous is changing at the rate of $0.605\ (t_{aT} + t_{aR})$ NM /hr. Because the variance of the random walk filter model is $q_y(t-t_o)$, a value of q_y also equal to $0.605\ (t_{aT} + t_{aR})$ would result in a filter model changing variance at about the same rate.

For a relatively long, combined airborne time at rendezvous of 15 hours, $q_y = 2.52 \times 10^{-3} NM^2/sec$.

Measurement Model

For the tree state filter model, Eq(14) simplifies to

$$d_T(t_i) = \sqrt{\{x(t_i) - x_T(t_i)\}^2 + \{y(t_i) - y_T(t_i)\}^2 + a_o^2} + v(t_i) \quad (27)$$

$$z(t_i) = h(\underline{x}(t_i), t_i) + v(t_i)$$

Since this is a simplification of the truth model, a suitable variance for the white noise, v, will also have to be found through trial and error. Primarily, v is replacing b + n, so a reasonable first guess is to set

$$R = \sigma_b^2 + \sigma_n^2$$

For the variances of b and n used in the truth model, the initial filter value of R is calculated to be 0.101 NM^2

Initialization

The tanker starts the filter initialization process by estimating v_R, v_{wx}, and v_{wy} - the receiver's true airspeed and the components of wind affecting its ground velocity. These would be calculated from the planned indicated airspeed for the receiver; INS computed ground speed, track, and heading; and CADC measured altitude and air temperature. The receiver's drift is then estimated from Eq(2). Or, if the receiver has readouts of any of those values onboard, they can be relayed

over the radio and inserted manually into the computer. The best guess of the receiver's x velocity, then, is $-v_R \cos\delta + v_{wx}$; and estimated deviation from this value, $\hat{v}_{xe}(0)$, is zero.

The tanker then calculates and attempts to fly the correct offset. If no radar aiding is used, $\hat{y}(0) = 0$. If an estimate of the lateral distance between the two aircraft, $\Delta\hat{y}_o$, is made with the help of radar or other means, then it is manually inserted and $\hat{y}(0) = y_T(0) + \Delta\hat{y}_o$.

The initial covariance matrix values are also tuned for best performance. Since $\underline{P}$ is symmetric, only upper triangular elements are calculated. The initial variance for y can be taken directly from the truth model: $P_{33}(0) = \sigma^2_{yo}$. Also, because $v_{xe} = v_{xc} + v_{xf}$, it would make sense to choose $P_{22}(0) = \sigma^2_{vxc} + \sigma^2_{vxf}$. The tanker would initially have very little information about the correlation of x,y, and v_{xc}, so $P_{12}(0)$ and $P_{23}(0)$ are set to zero.

The only initial conditions not yet specified are $\hat{x}(0)$, $P_{11}(0)$, and $P_{13}(0)$. A TACAN measurement at t=0 can be used to approximate those values. Approximate mean and covariance relations are derived using a Taylor series expansion about $\hat{y}(0)$ and the initial TACAN measurement.

The actual distance, d, is related to x, y, and a by

$$d = \sqrt{(x-x_T)^2 + (y-y_T)^2 + a^2}$$

The effects of altitude deviations from a_o are ignored, as discussed earlier, and the equation above is rearranged to form

a function $\Delta x(d,\Delta y)$:

$$\Delta x(d,\Delta y) = \sqrt{d^2 - \Delta y^2 - a_o^2} \tag{28}$$

where $\Delta x = x - x_T$ and $\Delta y = y - y_T$. Now Eq(27) is expanded to first order about $\Delta x_o = \Delta x(d_T, \Delta\hat{y})$ where d_T is the TACAN measured distance, and $\Delta\hat{y} = \hat{y} - y_T$:

$$\Delta x(d,\Delta y) = \Delta x_o + \frac{\partial \Delta x}{\partial d}\Bigg|_{\substack{d = d_T \\ \Delta y = \Delta\hat{y}}} (d - d_T) + \frac{\partial \Delta x}{\partial \Delta y}\Bigg|_{\substack{d = d_T \\ \Delta y = \Delta\hat{y}}} (\Delta y - \Delta\hat{y}) \tag{29}$$

$d - d_T$ is the TACAN error, d_e; and $\Delta y - \Delta\hat{y} = (y - y_T) - (\hat{y} - y_T) = y - \hat{y}$ which is the cross-track error y_e. The derivatives are evaluated and Eq(29) reduces to

$$\Delta x(d,\Delta y) = \Delta x_o + \frac{d_T}{\Delta x_o} d_e - \frac{\Delta\hat{y}}{\Delta x_o} y_e \tag{30}$$

Now $\hat{x}(0)$, $P_{11}(0)$, and $P_{13}(0)$ can be approximated to first order by taking the appropriate expected values and making use of Eq(30). Remember that d_T and Δx_o are not random, and that d_e and y_e are assumed to be zero mean and independent.

$\hat{x}(0)$:

$$x = x_T + \Delta x$$

$$= x_T + \Delta x_o + \frac{d_T}{\Delta x_o} d_e - \frac{\Delta\hat{y}}{\Delta x_o} y_e$$

$$\hat{x} = x_T + \Delta x_o + \frac{d_T}{\Delta \bar{x}_o} \; E\{d_e\} - \frac{\Delta \hat{y}}{\Delta x_o} \; E\{y_e\}$$

$$\hat{x}(0) = x_T(0) + \Delta x_o(0) \tag{31}$$

$P_{11}(0)$:

$$x - \hat{x} = (x_T + \Delta x) - (x_T + \Delta \hat{x})$$

$$= \Delta x - \Delta \hat{x}$$

$$= (\Delta x_o + \frac{d_T}{\Delta x_o} \; d_e - \frac{\Delta \hat{y}}{\Delta x_o} \; y_e) - (\hat{x} - x_T)$$

$$= \frac{d_T}{\Delta x_o} \; d_e - \frac{\Delta \hat{y}}{\Delta x_o} \; y_e$$

$$P_{11} = E\{(x - \hat{x})^2\}$$

$$= \frac{d_T^2}{\Delta x_o^2} \; E\{d_e^2\} - 2 \; \frac{d_T \Delta \hat{y}}{\Delta x_o^2} \; E\{d_e y_e\}$$

$$+ \frac{\Delta \hat{y}^2}{\Delta x_o^2} \; E\{y_e^2\}$$

$$P_{11}(0) = \frac{1}{\Delta x_o^2(0)} \{d_T^2(0)(\sigma_b^2 + \sigma_n^2) + \Delta \hat{y}^2(0) \sigma_{yo}^2\} \tag{32}$$

$P_{13}(0)$:

$$P_{13} = E\{(x - \hat{x})(y - \hat{y})\}$$

$$= E\{(\frac{d_T}{\Delta x_o} d_e - \frac{\Delta \hat{y}}{\Delta x_o} \; y_e) \; y_e\}$$

$$= \frac{d_T}{\Delta x_o} \; E\{d_e \; y_e\} - \frac{\Delta \hat{y}}{\Delta x_o} \quad E\{y_e^2\}$$

$$P_{13}(0) = \frac{-\Delta \hat{y}(0)\sigma_{yo}^2}{\Delta x_o(0)} \tag{33}$$

Propagation

Given the simplified filter dynamics model of Eq (26), the state transition matrix is

$$\underline{\Phi}(t_i, t_{i-1}) = \begin{bmatrix} 1 & (t_i - t_{i-1}) & 0 \\ 0 & 1 & 0 \\ 0 & 0 & 1 \end{bmatrix} \tag{34}$$

For a sample time of $\Delta t_i = t_i - t_{i-1}$, the filter propagation equations, (19) and (20), can be written as follows:

$$\hat{\underline{x}}(t_i^-) = \begin{bmatrix} 1 & \Delta t_i & 0 \\ 0 & 1 & 0 \\ 0 & 0 & 1 \end{bmatrix} \hat{\underline{x}}(t_{i-1}^+)$$

$$+ \int_{t_{i-1}}^{t_i} \begin{bmatrix} 1 & (t_i - \tau) & 0 \\ 0 & 1 & 0 \\ 0 & 0 & 1 \end{bmatrix} \begin{bmatrix} -v_R \cos\delta + v_{wx} \\ 0 \\ 0 \end{bmatrix} d\tau$$

which reduces to

$$\underline{x}(t_i^-) = \begin{bmatrix} \hat{x}(t_{i-1}^+) + (\hat{v}_{xe}(t_{i-1}^+) - v_R \cos\delta + v_{wx})\Delta t_i \\ v_{xe}(t_{i-1}^+) \\ y(t_{i-1}^+) \end{bmatrix} \tag{35}$$

And,

$$\underline{P}(t_i^-) = \begin{bmatrix} 1 & \Delta t_i & 0 \\ 0 & 1 & 0 \\ 0 & 0 & 1 \end{bmatrix} \underline{P}(t_{i-1}^+) \begin{bmatrix} 1 & 0 & 0 \\ \Delta t_i & 1 & 0 \\ 0 & 0 & 1 \end{bmatrix}$$

$$\int_{t_{i-1}}^{t_i} \begin{bmatrix} 1 & (t_i-\tau) & 0 \\ 0 & 1 & 0 \\ 0 & 0 & 1 \end{bmatrix} \begin{bmatrix} 0 & 0 & 0 \\ 0 & q_x & 0 \\ 0 & 0 & q_y \end{bmatrix} \begin{bmatrix} 1 & 0 & 0 \\ (t_i-\tau) & 1 & 0 \\ 0 & 0 & 1 \end{bmatrix} d\tau$$

Since $\underline{P}$ is symmetric, only the upper triangular elements need to be calculated. The matrix equation above reduces to the following relations:

$$P_{11}^- = P_{11} + 2\,P_{12}\Delta t_i + P_{22}\,\Delta t_i^2 + \tfrac{1}{3} q_x\,\Delta t_i^3 \qquad (36a)$$

$$P_{12}^- = P_{12} + P_{22}\Delta t_i + \tfrac{1}{2}\, q_x\,\Delta t_i^2 \qquad (36b)$$

$$P_{22}^- = P_{22} + q_x\,\Delta t_i \qquad (36c)$$

$$P_{13}^- = P_{13} + P_{23}\,\Delta t_i \qquad (36d)$$

$$P_{13}^- = P_{23} \qquad (36e)$$

$$P_{33}^- = P_{33} + q_y\,\Delta t_i \qquad (36f)$$

where the P terms on the right are the upper triangular elements of $\underline{P}(t_{i-1}^+)$, and the P^- terms are elements of $\underline{P}(t_i^-)$.

Update

From the filter measurement model, Eq(27),

$$h\{\underline{x}(t_i)\} = \{[x(t_i) - x_T(t_i)]^2 + [y(t_i) - y_T(t_i)]^2 + a_o^2\}^{\frac{1}{2}}$$

$$= \sqrt{\Delta x(t_i)^2 + \Delta y(t_i)^2 + a_o^2} \qquad (37)$$

Then, from Eq(26),

$$\underline{H}(t_i) = \left. \frac{\partial h\{\underline{x}(t_i)\}}{\partial \underline{x}} \right|_{\underline{x} = \hat{\underline{x}}}$$

$$= \left[\frac{\Delta\hat{x}(t_i)}{d_f(t_i)} \quad 0 \quad \frac{\Delta\hat{y}(t_i)}{d_f(t_i)} \right] \tag{38}$$

where d_f is the filter computed distance

$$d_f(t_i) = \sqrt{\Delta\hat{x}(t_i)^2 + \Delta\hat{y}(t_i)^2 + a_o^2}$$

The state and covariance updates are now just a straightforward application of equations (21) through (25). The resulting update relations are listed in the next section.

Sometimes when measurements are nonlinear, filter performance can be improved by adding a bias correction term to the predicted measurement value, $h(\hat{\underline{x}})$ (Ref 12: 225). For a single measurement, the appropriate bias correction is given by

$$b_c = \tfrac{1}{2}\, \mathrm{tr}\left[\frac{\partial^2 h(\hat{\underline{x}})}{\partial \underline{x}^2} \quad \underline{P} \right]$$

The correction term for this problem is then found to be

$$b_c = \tfrac{1}{2}\{ \left(\frac{1}{d_f} - \frac{\Delta\hat{x}^2}{d_f^3} \right) P_{11} + \left(\frac{1}{d_f} - \frac{\Delta\hat{y}^2}{d_f^3} \right) P_{33} \} \tag{39}$$

Now the predicted measurement value for forming the residual in Eq(22) is

$$z(t_i) = h\{\hat{\underline{x}}(t_i)\} + b_c(t_i)$$

In effect, z was just estimated by expanding $h(\underline{x})$ to second order and taking the expected value. Eq(22) now becomes

$$\delta\hat{\underline{x}}\ (t_i^+) = \underline{K}(t_i)\ \{z(t_i) - \hat{z}(t_i)\} \tag{40}$$

Estimation Algorithm

The entire estimation algorithm is now summarized. Anytime prior to rendezvous, CP coordinates, rendezvous true course, receiver indicated airspeed, and a_o are loaded into tanker's navigation computer. At each measurement time, INS computed tanker position is transformed to the coordinate system illustrated in Figure 2 on page 10.

At start of rendezvous:

1. INS and CADC data are used to compute v_R, v_{wx}, v_{wy}, and

$$\delta = \sin^{-1}\left[\frac{v_{wy}}{v_R}\right]$$

2. $u = -v_R \cos\delta + v_{wx}$

3. Tanker computes and attempts to establish correct offset.

Initialization:

1. If an estimate of the receiver's actual offset can be obtained from radar or other means, $\Delta\hat{y}(0)$ is inserted manually. If no update is made, $\Delta\hat{y}(0)$ equals desired offset.
2. The filter is started with an initial TACAN measurement, $d_T(0)$.
3. $\hat{\underline{x}}$ and $\underline{P}$ are initialized as follows. The time argument for

all variables is t=0.

$$\Delta\hat{x} = \sqrt{d_T^2 - \Delta\hat{y}^2 - a_o^2}$$

$$\hat{x} = x_T + \Delta\hat{x}$$

$$\hat{v}_{xe} = 0$$

$$\hat{y} = y_T + \Delta\hat{y}$$

$$P_{11} = \frac{1}{\Delta\hat{x}^2}\left[d_T^2\,(\sigma_b^2 + \sigma_n^2) + \Delta\hat{y}^2\,\sigma_{yo}^2\right]$$

$$P_{12} = 0$$

$$P_{22} = \sigma_{vxc}^2 + \sigma_{vxf}^2$$

$$P_{13} = -\frac{\Delta\hat{y}}{\Delta\hat{x}}\,\sigma_{yo}^2$$

$$P_{23} = 0$$

$$P_{33} = \sigma_{yo}^2$$

Propagation:

$\underline{\hat{x}}$ and $\underline{P}$ are propagated from sample time t_{i-1} to t_i with the following equations. Minus superscripts indicate t_i^- values, the variables on the right side of the equations are t_{i-1}^+ values.

$$\Delta t = t_i - t_{i-1}$$

$$\hat{x}^- = \hat{x} + (\hat{v}_{xe} + u)\Delta t_i$$

$$\hat{v}_{xe}^- = \hat{v}_{xe}$$

$$\hat{y}^- = \hat{y}$$

$$P_{11}^- = P_{11} + 2P_{12}\Delta t_i + P_{22}\Delta t_i^2 + \frac{1}{3} q_x \Delta t_i^3$$

$$P_{12}^- = P_{12} + P_{22}\Delta t_i + \frac{1}{2} q_x \Delta t_i^2$$

$$P_{22}^- = P_{22} + q_x \Delta t_i$$

$$P_{13}^- = P_{13} + P_{23}\Delta t_i$$

$$P_{23}^- = P_{23}$$

$$P_{33}^- = P_{33} + q_y \Delta t_i$$

Update:

At each sample time, a TACAN measurement d_T is used to update $\underline{\hat{x}}$ and $\underline{P}$. The following relations are derived from equations (21) through (25) with a bias correction term added. $\underline{\hat{x}}$ and $\underline{P}$ elements on the right side of the equations are t_i^- values.

$$\Delta\hat{x} = \hat{x} - x_T$$

$$\Delta\hat{y} = \hat{y} - y_T$$

$$d_f = \sqrt{\Delta\hat{x}^2 + \Delta\hat{y}^2 + a_o^2}$$

$$H_1 = \Delta\hat{x}/d_f$$

$$H_2 = 0$$

$$H_3 = \Delta\hat{y}/d_f$$

$$A = H_1^2 P_{11} + 2H_1 H_3 P_{13} + H_3^2 P_{33} + R$$

$$PH_1 = H_1 P_{11} + H_3 P_{13}$$

$$PH_2 = H_1 P_{12} + H_3 P_{23}$$

$$PH_3 = H_1 P_{13} + H_3 P_{33}$$

$$K_1 = PH_1/A$$

$$K_2 = PH_2/A$$

$$K_3 = PH_3/A$$

$$b_c = \tfrac{1}{2}\{(1/d_f - \Delta\hat{x}^2/d_f^3)P_{11} + (1/d_f - \Delta\hat{y}^2/d_f^3)P_{33}\}$$

$$\hat{z} = d_f + b_c$$

$$r = d_T - \hat{z}$$

$$\hat{x}^+ = \hat{x} + K_1 r$$

$$\hat{v}_{xe}^+ = \hat{v}_{xe} + K_2 r$$

$$\hat{y}^+ = \hat{y} + K_3 r$$

$$P_{11}^+ = P_{11} - K_1 PH_1$$

$$P_{12}^+ = P_{12} - K_1 PH_2$$

$$P_{22}^+ = P_{22} - K_2 PH_2$$

$$P_{13}^+ = P_{13} - K_1 PH_3$$

$$P_{23}^+ = P_{23} - K_2 PH_3$$

$$P_{33}^+ = P_{33} - K_3 PH_3$$

This algorithm is used to continually propagate and update the receiver's state estimate for as long as needed by the controller.

V Control

Algorithms were developed to calculate the correct offset distance, the appropriate time for the tanker to start its turn, and bank angle commands during the turn. For this initial feasibility study, the control laws are based on a deterministic dynamics model with the current receiver state estimate as input.

Tanker Dynamics

Eq(1) is appropriate for deriving the kinematic relations for the tanker as it was for the receiver:

$$\underline{v} = \underline{v}_{a/w} + \underline{v}_w$$

where $\underline{v}$ is velocity relative to the ground, $v_{a/w}$ is the velocity of the aircraft with respect to the air mass, and $\underline{v}_w$ is the velocity of the wind. The tanker's heading, Ψ, is measured counter - clockwise from the positive x axis as shown back in Figure 2. Then for a tanker true airspeed of v_T, the components of $\underline{v}_{a/w}$ are

$$v_{a/wx} = v_T \cos \Psi$$

$$v_{a/wy} = v_T \sin \Psi$$

The components of the tanker's velocity in the pseudo ground fixed frame of the INS are therefore

$$v_{Tx} = v_T \cos \Psi + v_{wTx} \tag{41}$$

$$v_{Ty} = v_T \sin \Psi + v_{wTy} \tag{42}$$

where v_{wTx} and v_{wTy} are the components of wind at the tanker's current position.

A simplified free body diagram of a KC-135 in a left turn, with positive left bank angle ϕ, is shown in Figure 3. L is lift, m the tanker's mass, and g the acceleration due to gravity. In a level turn, the vertical component of lift balances the weight, mg, so

$$L \cos \phi - mg = 0 \tag{43}$$

In a turn, the tanker has a centripetal acceleration, $\dot{\Psi} v_T$, which is caused by the horizontal component of lift. The resulting equation of motion is

$$L \sin \Psi = m\dot{\Psi} v_T \tag{44}$$

Equations (43) and (44) are now combined to form a relation for $\dot{\Psi}$:

$$\dot{\Psi} = \frac{g \tan\phi}{v_T} \tag{45}$$

Some simplifications were employed in developing this model, but these equations represent the principle dynamic effects throughout the turn. The air mass and INS coordinate frame are assumed to be non-accelerating, which they virtually are when compared to the accelerations of a turning aircraft. Also, the velocity vector is assumed to be along the tanker's longitudinal body axis. For a KC-135 at cruise airspeed and shallow bank angles, the angle of attack is small; and its effect on bank and heading calculations is assumed to be negligible for the purposes of this problem. As in the filter design, an implementable control law has to be based on a model of just the dominant effects.

Turn Point

The geometry of the tanker's turn is illustrated in Figure 4. For a constant bank angle, constant airspeed turn, the tanker's flight path relative to the air mass is circular with radius of turn

$$r_T = \frac{v_T}{\dot{\psi}} \tag{46}$$

The tanker wants to roll out on the refueling track with zero lateral drift. Then, as the receiver did, it needs to apply a drift correction; and its final heading will be

$$\Psi_f = \pi + \delta$$

where

$$\delta = \sin^{-1}\left[\frac{v_{wTy}}{v_T}\right] \tag{47}$$

From any initial heading, Ψ_o, the change in the tanker's position during the turn will equal the change in position within the air mass plus the change due to movement of the air mass over the ground. Then

$$\begin{aligned}\Delta x_T &= x_{Tf} - x_{To} \\ &= r_T\left[\sin(\pi+\delta) - \sin\Psi_o\right] + v_{wTx}T \\ &= r_T\left[-\sin\delta - \sin\Psi_o\right] + v_{wTx}T \end{aligned} \tag{48}$$

where x_{Tf} and x_{To} are the tanker final and initial x coordinates and T is the duration time of the turn. T can be found from

$$T = \frac{\Delta\Psi}{\dot{\psi}} = \frac{\pi+\delta-\Psi_o}{\dot{\psi}} \tag{49}$$

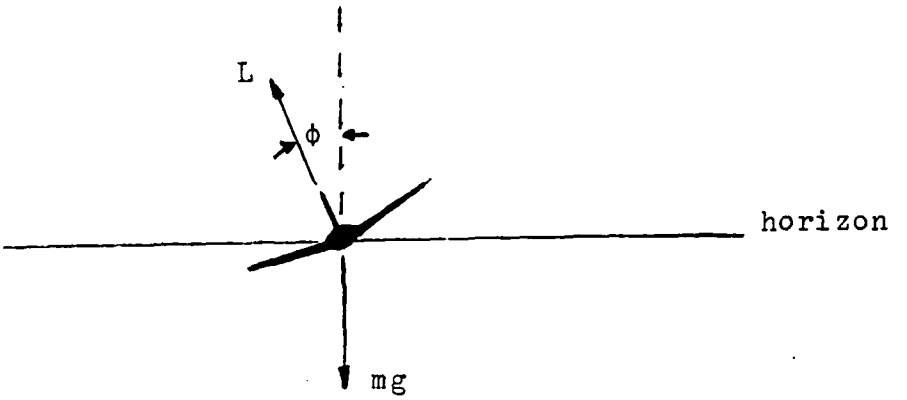

Figure 3. Tanker Free Body Diagram (Tail-on view)

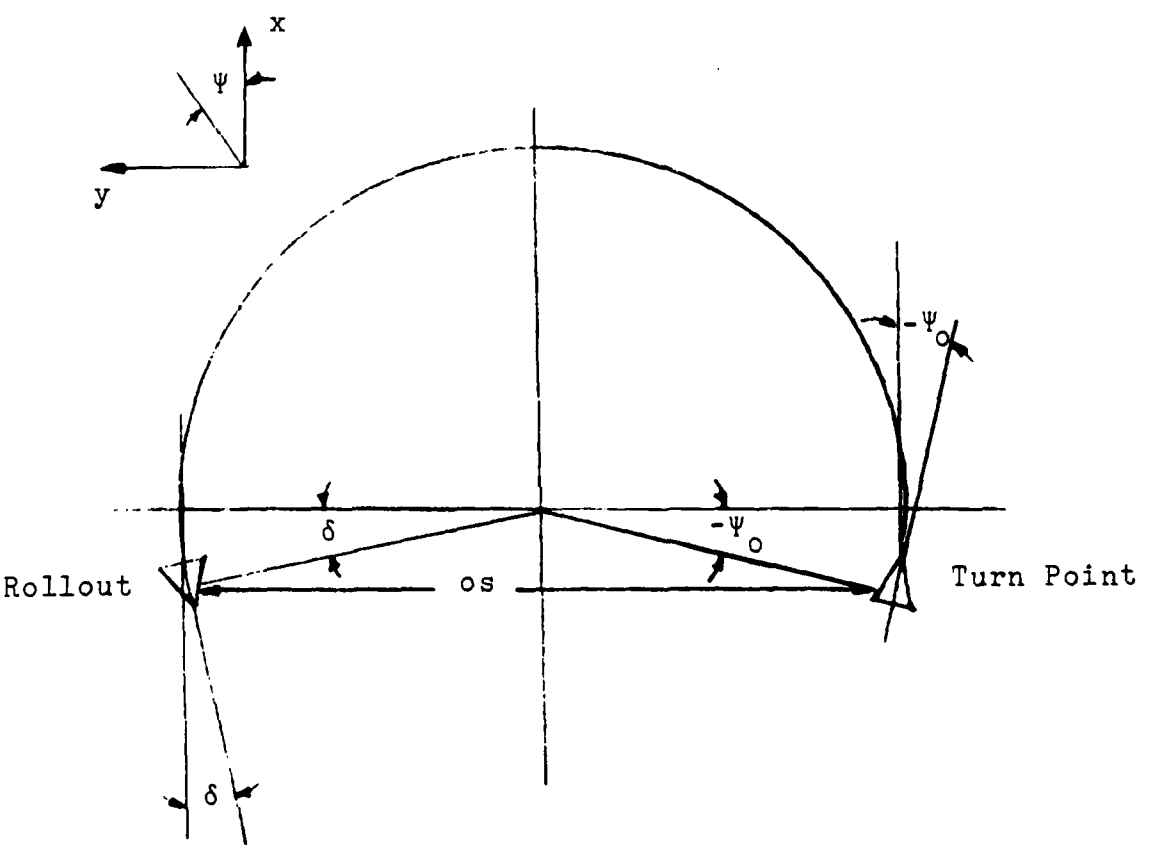

Figure 4. Rendezvous Turn Geometry

By substituting Eq(45) into Eq(46), it is found that

$$r_T = \frac{v_T}{g \tan \phi} \tag{50}$$

Also, substituting Eq(45) into Eq(49) results in

$$T = \frac{\Delta\Psi \; v_T}{g \tan \phi} \tag{51}$$

Now these relations for r_T and T are used in Eq(48) to derive

$$\Delta x_T = \frac{v_T}{g \tan\phi} \{ v_T(-\sin \delta - \sin \Psi_o) + (\pi + \delta - \Psi_o) \; v_{wTx} \} \tag{52}$$

Similarly, it can be shown that

$$\Delta y_T = y_{Tf} - y_{To}$$

$$= r_T \left[\cos \delta + \cos \Psi_o\right] + v_{wTy} T \tag{53}$$

$$= \frac{v_T}{g \tan \phi} \{v_T(\cos \delta + \cos \Psi_o) + (\pi + \delta - \Psi_o) v_{wTy}\} \tag{54}$$

Eq(54) can be used directly to determine the nominal offset distance. For the tanker to fly towards the receiver parallel to the refueling track, a drift correction of $-\delta$ must be applied. The change in sign is because δ is calculated for the rollout heading, and the tanker is initially flying in the opposite direction. Then $\Psi_o = -\delta$ and the desired offset is

$$os = \frac{v_T}{g \tan \phi_n} \{ 2v_T \cos \delta + (\pi + 2\delta) \; v_{wTy} \} \tag{55}$$

where ϕ_n is the nominal bank angle.

The present procedure uses a nominal bank angle of 30 degrees. But 30 degrees is also the tanker's maximum bank angle under normal conditions. Therefore, a shallower nominal bank angle must be used if bank angle corrections are to be applied during the turn. With no cross-wind, a nominal bank angle of 25 degrees requires about a 9.6 NM offset. Nominal offsets greater than that were considered unreasonable due to airspace restrictions imposed by air traffic control.

The tanker attempts to establish the nominal offset distance, but the computed time to turn should be based on the tanker's actual offset and heading - not the nominal. For example, the tanker may actually be wider than the computed offset and its initial heading other than $-\delta$ while it is correcting to course. In that case, it should turn earlier and with a shallower bank angle than nominal. The ability to compute other than nominal solutions does not exist with the present method but could be implemented with the proposed system.

To compute ϕ_r, the required bank angle to roll out along the receiver's estimated flight track, $\hat{y} - y_T$ is substituted for Δy_T and Eq(54) is solved for ϕ:

$$\phi_r = \tan^{-1}\left[\frac{v_T}{g(\hat{y}-y_T)}\{v_T(\cos\delta + \cos\Psi_o)+(\pi+\delta-\Psi_o)\ v_{wTy}\}\right] \quad (56)$$

Given ϕ_r, the time required for the turn is

$$T_r = \frac{(\pi+\delta-\Psi_o)\ v_T}{g\ \tan\phi_r} \tag{57}$$

which is derived from Eq(51). If the tanker turns at the current time, its x coordinate at rollout will be

$$x_{Tf} = x_T + \Delta x_T$$

where Δx_T is found from Eq(52). The receiver's position at tanker rollout is estimated by

$$\hat{x}_f = \hat{x} + \hat{v}_x\ T_r$$

where

$$\hat{v}_x = (-v_R \cos\delta + v_{wx}) + \hat{v}_{xe} \tag{58}$$

The tanker wants to roll out 2 NM in front of the receiver. If it turns too early, its miss distance in front of the receiver, $\hat{x}_m$, is

$$\hat{x}_m = \hat{x}_f - 2 - x_{Tf}$$

But $\hat{x}_m$ is decreasing at the rate of the two aircraft's closing speed, $v_{Tx}-\hat{v}_x$. The estimated time to go until the turn should be started, TTG, is then given by

$$TTG = \frac{\hat{x}_m}{v_{Tx} - \hat{v}_x} \tag{59}$$

TTG is counted down between updates, and the tanker turns with bank angle ϕ_r when TTG ≤ 0.

The algorithm for determining the turn point is now summarized:

A. The tanker computes and attempts to establish the correct offset for a nominal bank angle ϕ_n:

1. $\delta = \sin^{-1}\left[\frac{v_{wTy}}{v_T}\right]$

2. $os = \frac{v_T}{g \tan \phi_n} \{2v_T \cdot \cos\delta + (\pi + 2\delta)v_{wTy}\}$

B. The required bank angle and time to go until turn are updated based on actual tanker position and heading:

1. $\Delta\Psi = \pi + \delta - \Psi_o$ (60a)

2. $\phi_r = \tan^{-1}\left[\frac{v_T}{g(\hat{y} - y_T)} \{v_T(\cos\delta + \cos\Psi_o) + \Delta\Psi v_{wTy}\}\right]$ (60b)

3. $T_r = \frac{\Delta\Psi \cdot v_T}{g \tan \phi_r}$ (60c)

4. $\Delta x_T = \frac{v_T}{g \tan \phi_r} \{v_T(-\sin\delta - \sin\Psi_o) + \Delta\Psi \cdot v_{wTx}\}$ (60d)

5. $x_{Tf} = x_T + \Delta x_T$ (60e)

6. $\hat{v}_x = (-v_R \cos\delta + v_{wx}) + \hat{v}_{xe}$ (60f)

7. $\hat{x}_f = \hat{x} + \hat{v}_x T_r$ (60g)

8. $\hat{x}_m = \hat{x}_f - 2 - x_{Tf}$ (60h)

9. $TTG = \frac{\hat{x}_m}{v_{Tx} - \hat{v}_x}$ (60i)

Closed Loop Control

As was stated previously, one of the primary potential benefits of the proposed system is that it would enable the tanker to use closed loop control during the final turn to rendezvous.

The present procedure is entirely open loop: the tanker maintains a constant 30 degrees of bank until reaching the refueling heading. A simple improvement would be to apply cross-track control only. At each update time, the tanker would compute the required bank angle to roll out in front of the receiver using Eq(56). The result should be decreased cross-track error at rollout, which would mean less lateral maneuvering would be required of the receiver to complete the join-up.

Using bank angle control to minimize the along-track error also, is more complicated. That is because, in general, the tanker cannot get from its present position and heading to a zero error rollout condition with a constant bank angle. A method of solving the problem which was used in the simulations, is based on the following basic algorithm:

1. Compute ϕ_r to roll out on the receiver's estimated track.
2. Determine the x miss distance if ϕ_r is used.
3. Adjust ϕ_r based on x miss. If the tanker would roll out in front of the receiver, decrease the bank angle and vice-versa.

The basic idea, then, is to see if an exact solution exists from the present position and heading. If one does not, adjust the

bank angle to fly towards one.

The first two steps of this algorithm are solved by equations (60a) through (60h). The remaining question is then how much to correct ϕ_r. An ad hoc method was used based on the following insights. If the tanker would roll out in front of the receiver, it needs to fly a longer path to the rendezvous. Similarly, if it would roll out behind the receiver, more cuttoff and a more direct route should be flown. A measure of the effect of a bank angle change at the present position, is the change in arc length it would cause if held until rollout. The control law was then based on the following equation:

$$r_{Tc}\Delta\Psi - r_{Tr}\Delta\Psi = k\hat{x}_m \tag{61}$$

where r_{Tr} is the radius of turn for ϕ_r, $\hat{x}_m$ is the projected miss distance using ϕ_r, r_{Tc} is corrected radius of turn, and k is a proportionality constant which will be tuned for best performance. In other words, the arc length is increased by an amount proportional to the miss distance. When Eq(61) is rearranged, the equation for r_{Tc} is

$$r_{Tc} = \frac{k\hat{x}_m}{\Delta\Psi} + r_{Tr} \tag{62}$$

This law exhibits the following desirable characteristics. If $\hat{x}_m$ is zero, then ϕ_r is an exact solution and r_{Tc} equals r_{Tr}. The change in turn radius is proportional to $\hat{x}_m$, and inversely proportional to $\Delta\Psi$ - the further away the tanker is from rollout, the less correction needed.

Eq(61) also gives some insight into setting k. A value of k=1 would increase the arc length by the amount of $\hat{x}_m$. Since both aircraft are flying at about the same speed, if the tanker would maintain r_{Tc} until rollout, it would roll out at about the same time that the receiver would reach the rollout point based on ϕ_r. A good initial trial value for k would then be 1.

The ad hoc control algorithm is then:

1. - 7. Same as equations (60a) through (60h).

8. $$r_{Tr} = \frac{v_T^2}{g \tan \phi_r}$$

9. $$r_{Tc} = r_{Tr} + \frac{k\hat{x}_m}{\Delta\Psi}$$

10. $$\phi_c = \tan^{-1}\left[\frac{v_T^2}{gr_{Tc}}\right]$$

At this point, the 30 degree maximum bank angle restriction should be recalled. For both the turn point and the closed loop bank angle control algorithms, the following conditional statement was added after step 2. (Eq(60b)):

2a. If $\phi_r \leq 30$ degrees, then set ϕ_r=30 degrees.

For the closed loop control algorithm, if ϕ_r is greater than 30 degrees, σ_c should also be set to 30 degrees and the algorithm stopped at that point. In that case, the tanker is headed for an overshoot of the desired rollout track: it cannot turn any tighter, and a shallower bank angle will only make the overshoot worse. Also, if y_T is greater than $\hat{y}$, the tanker has

already overshot the receiver's estimated cross-track position, and the full 30 degrees of bank should be used.

So far, a mathematical model of an air refueling rendezvous has been created, and estimation and control algorithms have been developed. The last major task of this study is to do an initial evaluation of the filter and controller designs.

VI Simulation Results

Computer simulations of a typical rendezvous were used for an initial analysis of the estimator and controller designs.

Simulation

The filter and controller were evaluated using Monte Carlo simulations. The statistics for each Monte Carlo run were calculated from the results of 30 separate, simulated rendezvous. In each rendezvous, a different set of random variable realizations was simulated.

The receiver's dynamics and the TACAN measurements were modelled exactly as described in the summary of Section III. The tanker's dynamics were modelled by Eqs(41), (42), and (45). In each case, the tanker started from a position along the minus y axis with an initial flight path direction parallel to the refueling track. v_R and v_T were both set to 396 knots, which would be typical for a refueling altitude of 25000 ft and standard day conditions.

SOFE (Ref 14) and SOFEPL (Ref 15), two computer programs developed for Monte Carlo simulations of Kalman filter design problems, were used to accomplish the runs and generate the appropriate outputs. The extended Kalman filter equations discussed in Section III are automatically implemented in SOFE with one exception. Rather than the standard update equations given by equations (21) through (25), a Carlson update (Ref 14: 28-29) is used. This type of update is algebraically equivalent to the standard form, but it has numerical stability and accuracy

advantages when used on a finite wordlength computer. Whether those advantages outweigh the inherent, increased computational requirements for this problem, would be an area for future study.

To ensure a standard means of comparison, the same control algorithms were used for all filter evaluations. The turn point algorithm given by Eqs(60a) through (60i), and the cross-track controller, which only uses Eq(56) at each update time, were used. Also, the control algorithms used the true state values rather than the estimated states as input. For the same reason, each controller was evaluated using the same filter algorithm to provide the estimated state inputs.

Filter

The big unanswered question about the proposed system is how much information can be gained from TACAN, distance-only measurements. Ideally, the filter would be so accurate that radar would not be needed. Then, accurate rendezvous could be conducted even if radar contact is lost or never achieved. The filter would be started as soon as the receiver passes the initial point. An accurate estimate of the receiver's cross-track position would then be used by the tanker to establish its initial offset. Unfortunately, though, the initial simulations indicated that attaining such a degree of accuracy may not be feasible.

A 7 state filter which modelled all of the states except the short correlation time component of TACAN error was initialized at simulated 100 NM ranges. The results indicated that, as suspected, some of the states were relatively unobservable.

The filter predicted error standard deviations, as measured by the square roots of the diagonal elements of $\underline{P}$, decreased very little for the TACAN bias, altimeter error, and constant v_{yc} states. Between the start and finish of the rendezvous, the predicted standard deviations only decreased about 10% for b, 1% for v_{yc}, and virtually not at all for a_e. Also, those slight improvements for b and v_{yc} did not occur until about the last 60 seconds of the rendezvous.

For an initial 100 NM range and σ_{yo} value of 6.15 NM, both the 7 state filter and the 3 state filter described in Section IV were very difficult to tune. The filters produced biased estimates; and they greatly overestimated their own accuracy: the diagonal elements of $\underline{P}$ quickly converged to values much less than the true error variances. An accurate cross-track estimate never could be achieved until the range decreased considerably. In Figure 5, the standard deviation of the filter's actual cross-track estimate error, computed for each sample time of a typical Monte Carlo run, is plotted. Notice that at t=310 seconds, which corresponds to about a 30 NM range, the actual filter error had a standard deviation of around 4 NM. The tanker would be better off using radar, with its assumed 1σ error of 1 NM at that range.

When it appeared that no progress was being made in designing an adequate estimator for that "worst case" situation, attention was shifted to a more restricted problem. It was assumed that the tanker would use radar to establish its offset

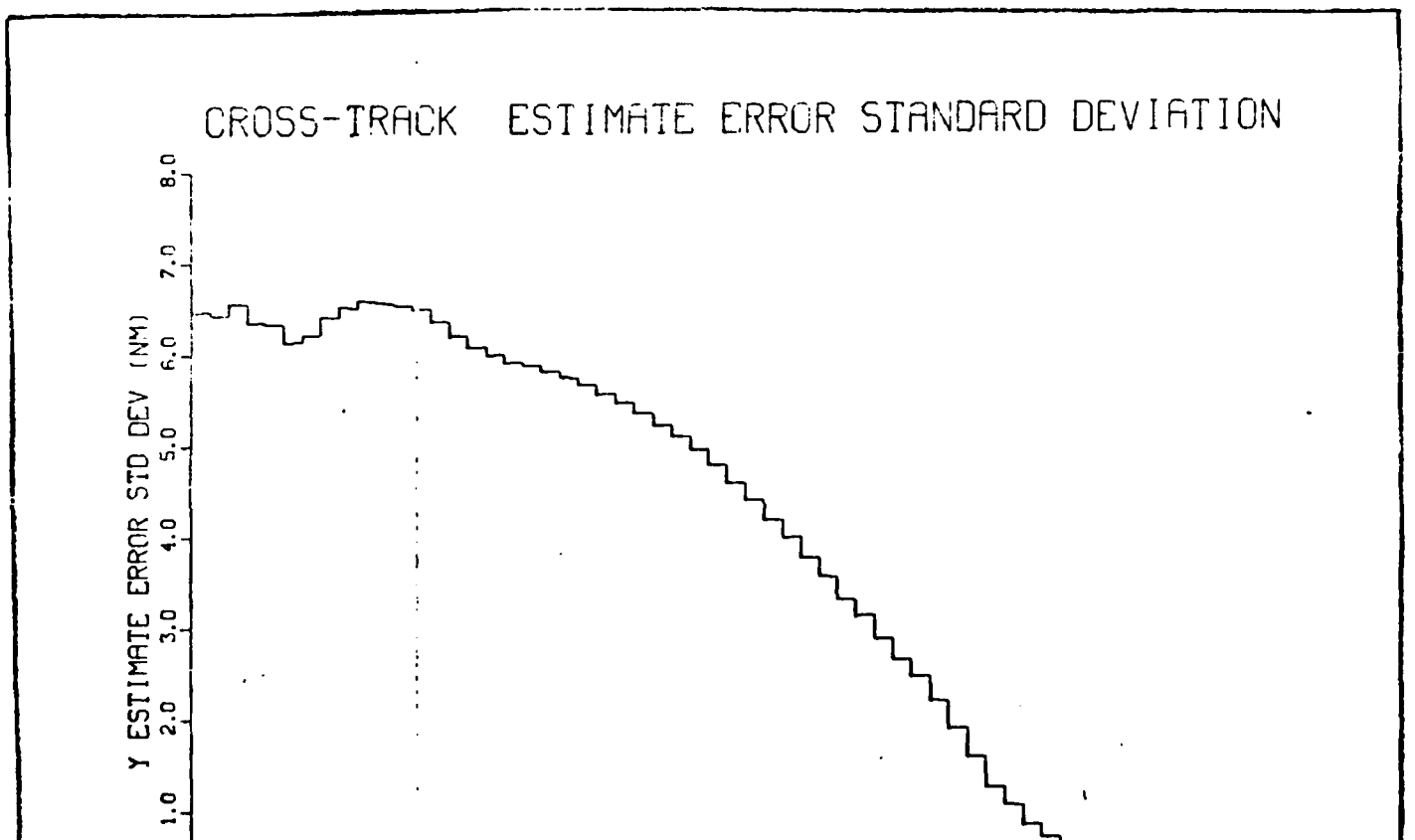

Figure 5. Standard Deviation of $\hat{y}$ Error for Non-Radar-Aided Rendezvous

and to obtain a relatively short range initial estimate of the receiver's position. The filter would then take over and propagate and update the state estimate through the rest of the rendezvous. The advantage of even this restricted case is that it would provide a state estimate for turn point calculations and bank angle control during the turn. The radar is good for initial estimates and positioning, but the one onboard the KC-135 cannot lock on a target. Therefore, it could not easily be used for periodic updating during the turn since all radar updates must be entered manually.

The filtering was initiated at a simulated range of 30 NM, giving about a 50 second period before reaching the turn point. This shorter range also makes the velocity assumptions about the receiver more valid. By 30 NM, the receiver should have completed any initial maneuvering or altitude changes that may have been necessary, and its flight path should be fairly stable.

The results of the 3 state filter simulations are plotted in Figures 6, 7, and 8. All of the filter parameters were tuned to the values discussed in Section IV. In each figure, the statistics of the actual filter error, computed from the time histories of 30 simulated rendezvous, are depicted. The actual filter error is defined as the difference between the appropriate truth state value and the filter estimated state value. The center, solid line represents the average error; the two broken lines are the mean error plus and minus the standard deviations; and the two dashed lines are the filter predicted standard

deviations, calculated as the average square root value of the appropriate diagonal element of $\underline{P}$.

Each of the plots demonstrate some desirable filter characteristics. The mean error stays near zero. Also, the filter predicted standard deviations fairly closely bracket the actual mean plus standard deviation plots. In other words, the filter performs its updates based on an internal model which closely approximates its actual performance.

The plots also indicate, however, that the accuracy does not improve significantly from the initial uncertainties. For the x position and velocity components, no noticeable improvement is made until about t=120 sec, which is when the tanker is approximately halfway through the turn. Meanwhile, the y estimate just exhibits a modest, steady improvement.

Some of the filter parameters were varied, but no noticeable improvement was achieved. For example, shorter sample periods were used. The results of Figures 6 to 8 were based on a simulated time between measurements of 10 sec. For Figures 9, 10, and 11, a shorter period of 2 sec was used. The actual error statistics stayed about the same.

Another interesting result was found when experimenting with the simulated TACAN errors. The TACAN bias error standard deviation of 0.1 is large compared to the short correlation time component's constant variance of 0.016 NM. However, if the bias error is removed entirely from both the truth and filter

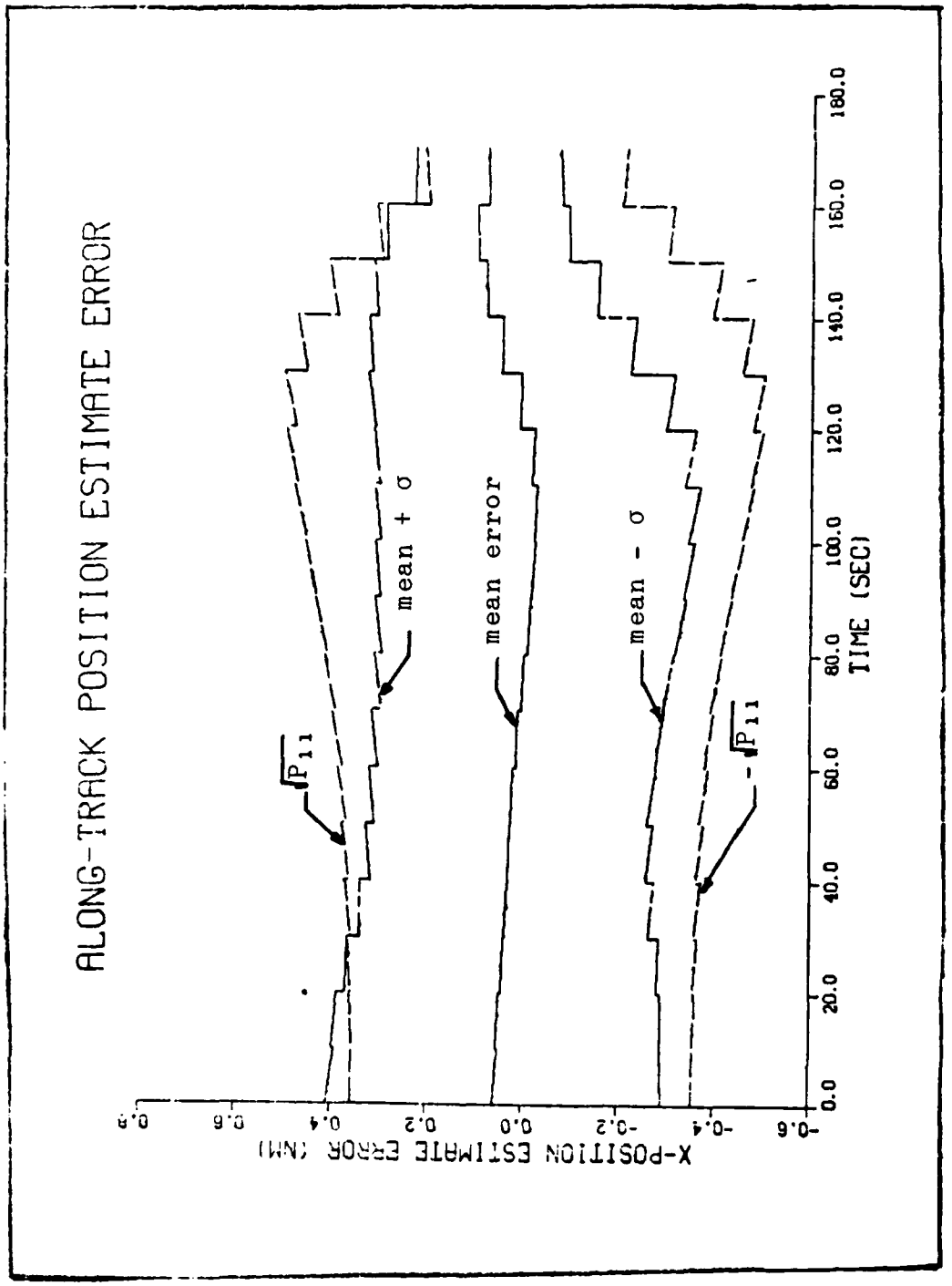

Figure 6. Actual and Predicted x Estimate Error Statistics

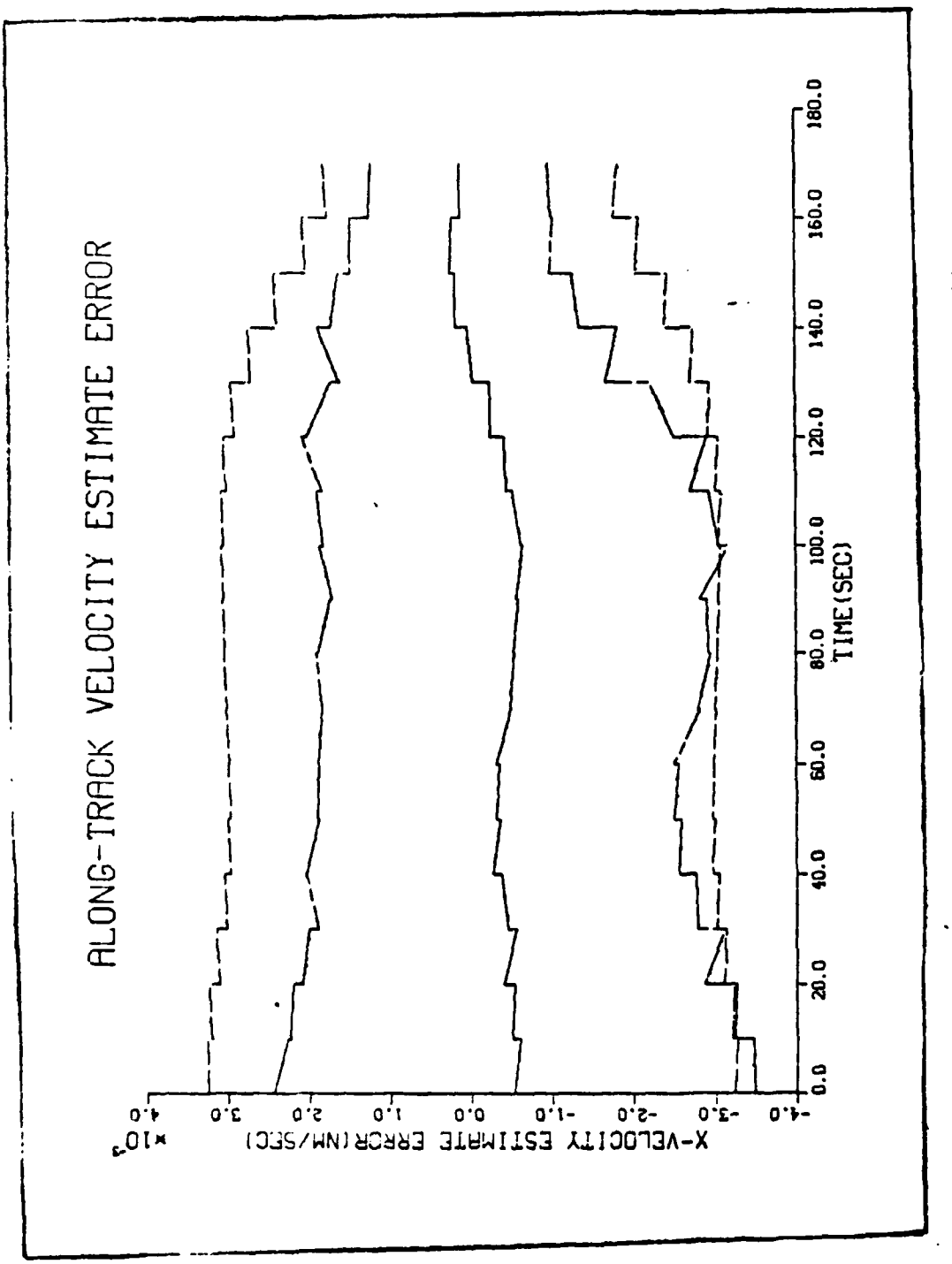

Figure 7. Actual and Predicted v_{xe} Estimate Error Statistics

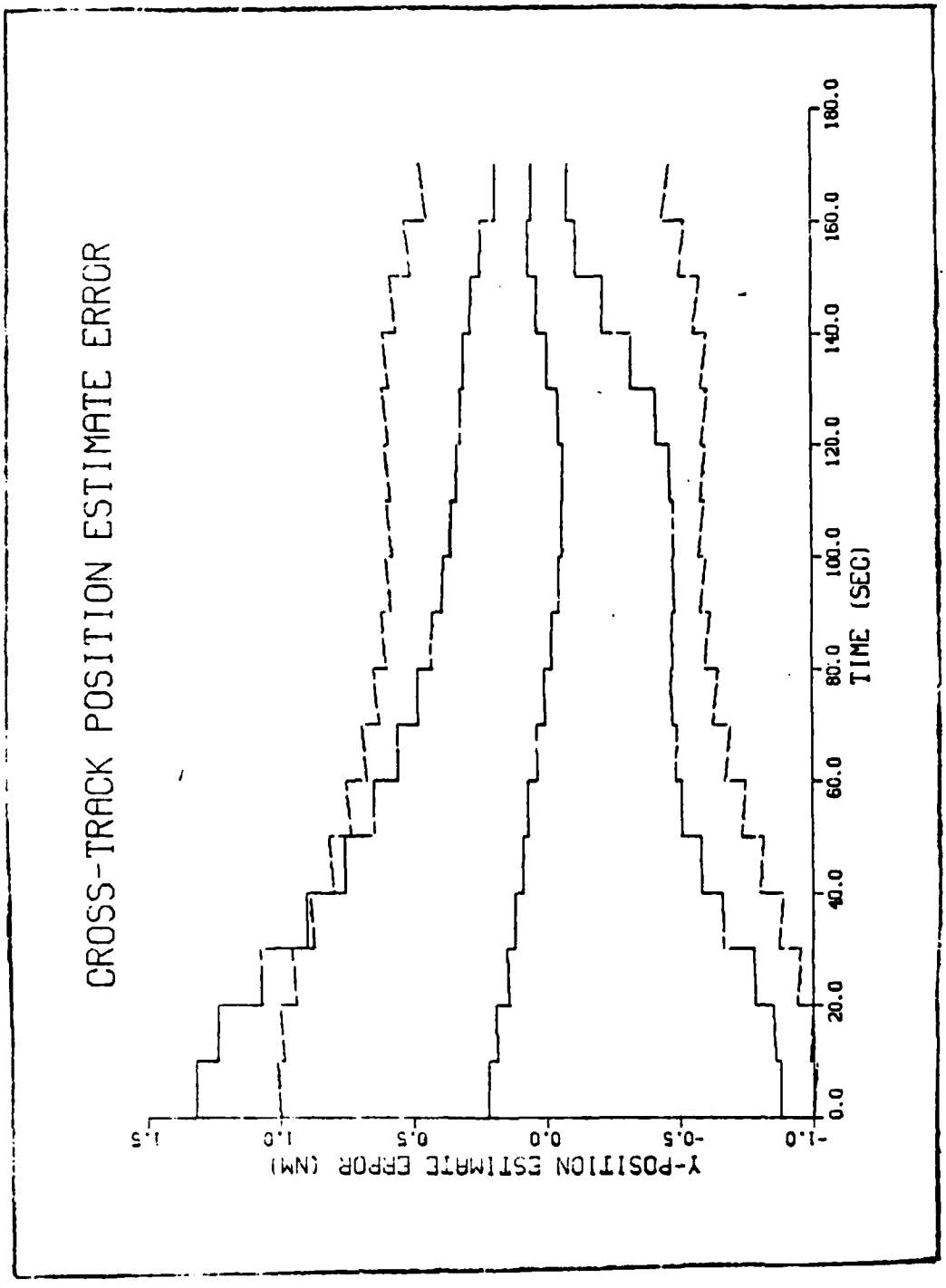

Figure 8. Actual and Predicted y Estimate Error Statistics

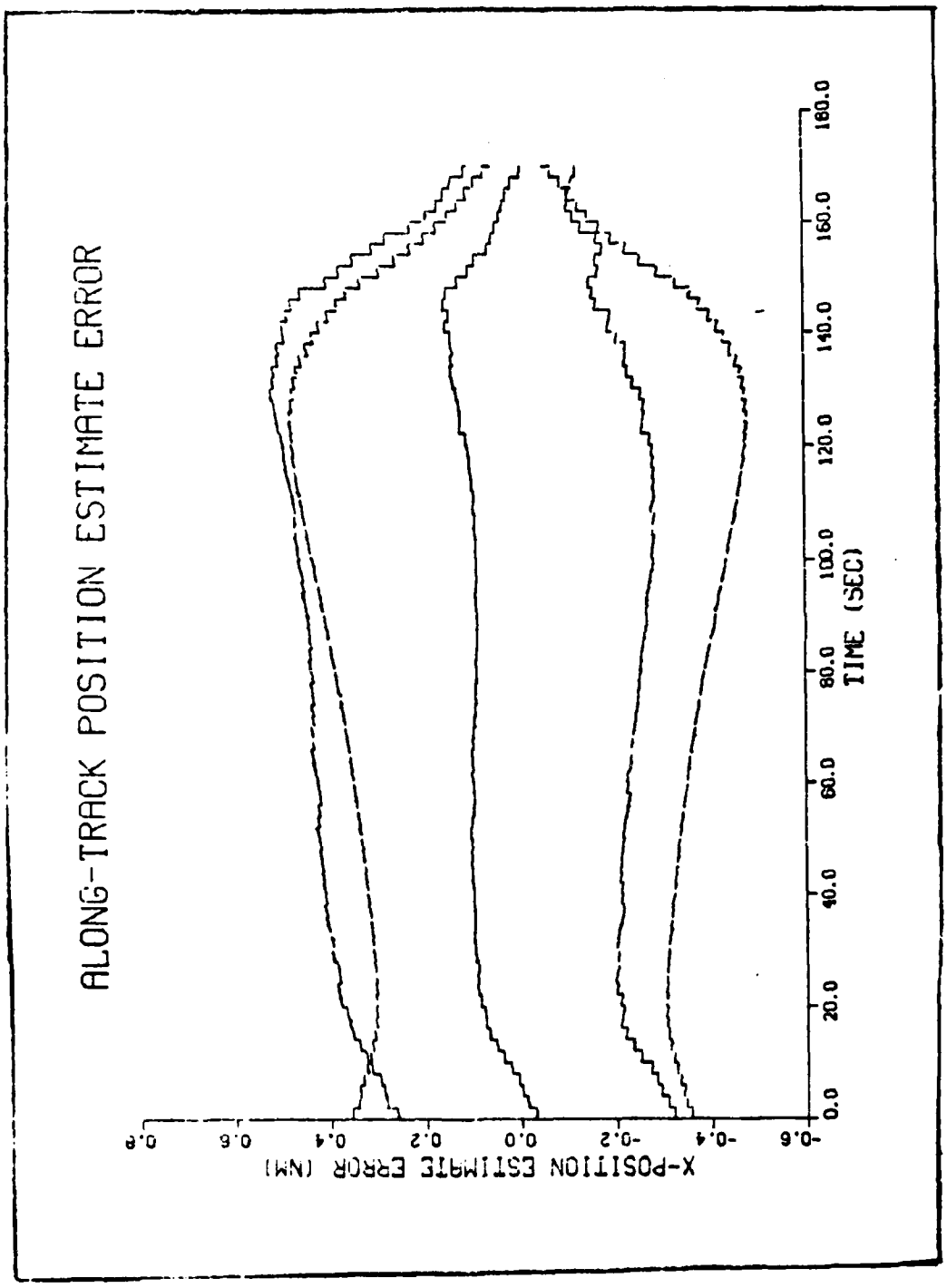

Figure 9. x Estimate Error Statistics-2 Sec Sample Period

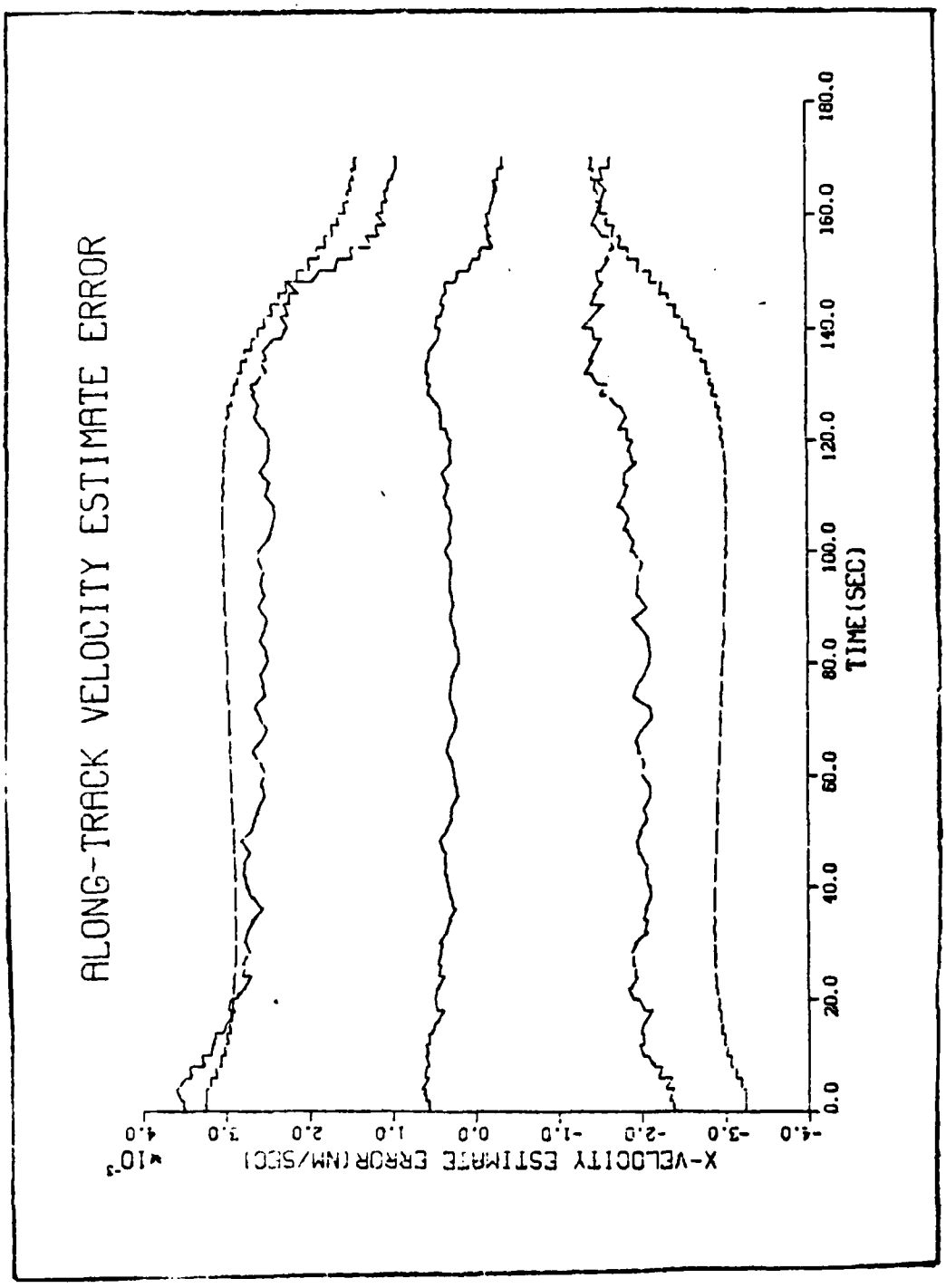

Figure 10. v_{xe} Estimate Error Statistics-2Sec Sample Period

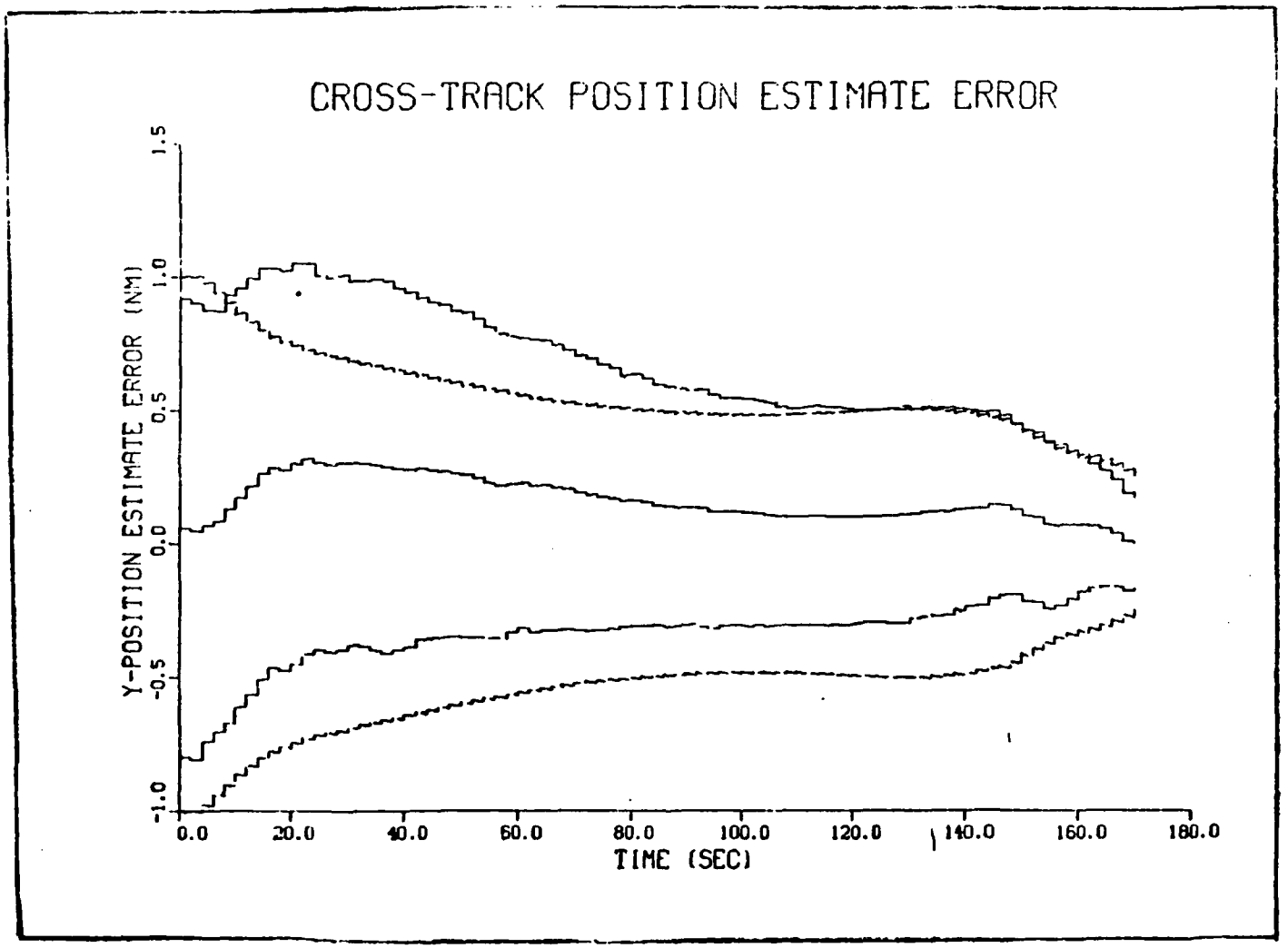

Figure 11. y Estimate Error Statistics-2 Sec Sample Period

models, the filter performance is still about the same. The cross-track error statistics for this case are plotted in Figure 12. The plots are almost identical to those in Figure 8. This result indicates that not much would be gained by being able to estimate b or calibrate it out of the TACAN.

All of the simulations seemed to indicate that the results plotted in Figures 6 to 8 represent a practical limit for the extended Kalman filter. The driving constraint on filter performance does not seem to be the number of filter states, the sample period, or the magnitude of the TACAN bias error. The rendezvous geometry itself, would intuitively seem to be the primary constraint. Because the aircraft are approaching each other nearly head-on, not much cross-track information is available until late in the rendezvous. Investigation of different rendezvous geometries might be a suitable area for future study.

The improvement in estimation accuracy over the initial uncertainties is not significant. But the extended Kalman filter does seem to be a relatively simple, stable method of generating a receiver state estimate up through completion of the rendezvous. With the present method, the tanker has no useful means of estimating the receiver's state once the turn is started.

Controller

The most important question of this study still remains to be answered: what improvement in rendezvous accuracy might be achieved with the proposed method? To answer that question, the

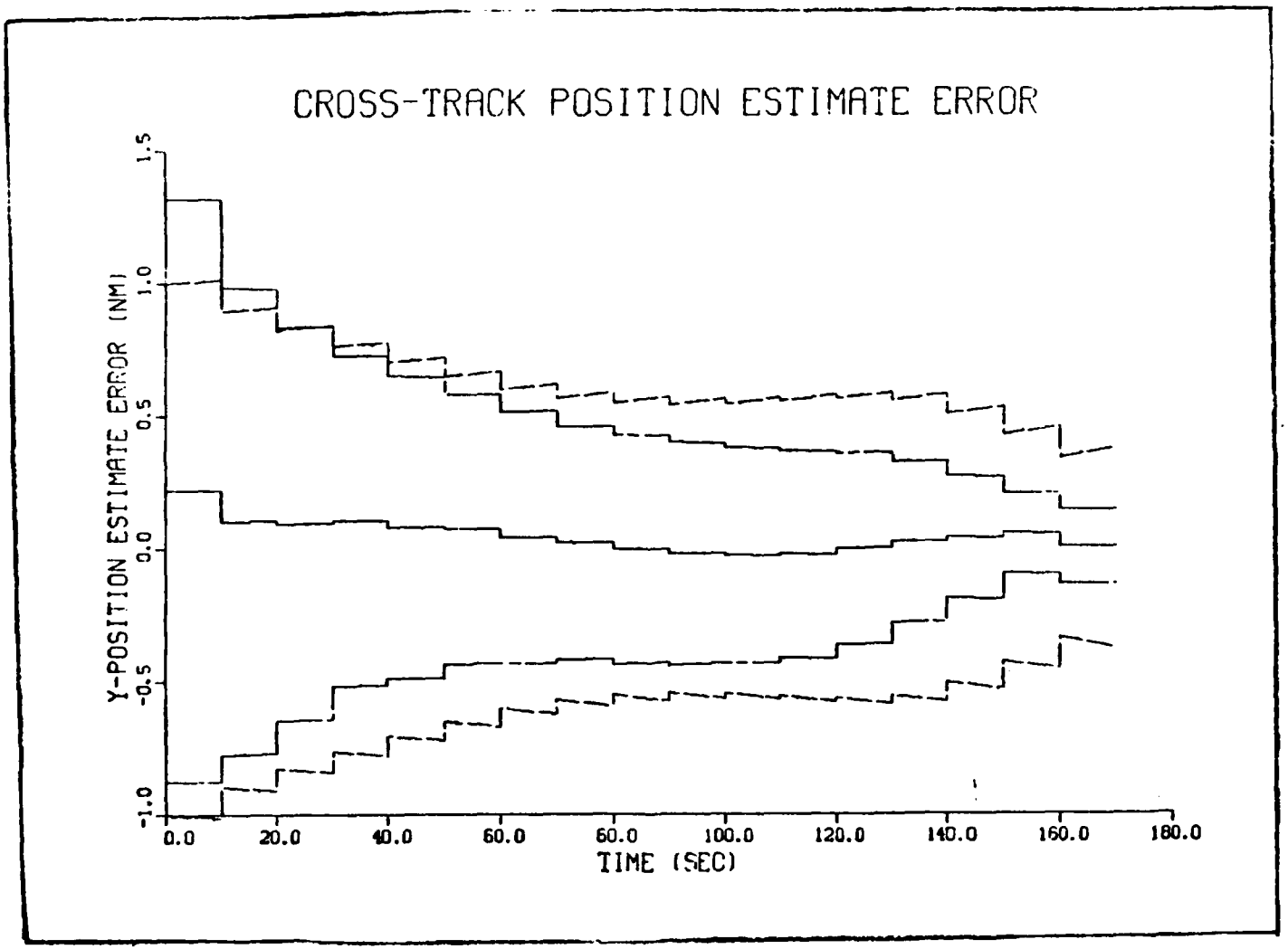

Figure 12. y Estimate Error Statistics-No TACAN Bias Error

control algorithms of Section V were incorporated into the Monte Carlo simulations. For each case studied, the 3 state filter with 10 second updates provided the inputs to the controller. Each rendezvous was initialized at a 30 NM range and was terminated when the tanker had turned to the refueling heading. The rollout errors were then calculated as

$$x_m = x(t_f) - 2 \text{ NM} - x_T(t_f)$$

$$y_m = y(t_f) - y_T(t_f)$$

where x_m and y_m are the rollout miss distances, x and y are the true receiver position coordinates, and t_f is the final, or rendezvous completion, time. For each Monte Carlo run, 30 simulated rendezvous were used to compute the means, standard deviations, and root mean square statistics for x_m and y_m.

To form a basis for comparison, the present rendezvous method was also simulated. For the airspeeds and zero wind conditions used in the simulations, the turn range chart (Ref 16: 3-5) gives a nominal offset of 7 NM and a turn range of 17 NM.

In the first case studied, it was assumed that the tanker had maneuvered to the computed offset distance, based on $\hat{y}$, prior to the turn. The only actual offset errors were then due to the $\hat{y}$ estimate errors. For the present, open loop method simulations, this meant that the tanker had established an estimated 7 NM offset, but the actual offset had a standard deviation of 1 NM due to radar estimate errors. For the controlled rendezvous, the tanker started from an estimated offset of 9.6 NM - the

nominal offset for a 25 degree bank turn. Again, the actual offset varied from this mean value with a 1σ error of 1 NM.

The results are listed in Table 1. Since the present method has no means of improving its estimate of the receiver's y position, its 1σ value for y_m is about equal to the initial radar estimate error. Also notice the large bias errors at rollout. These would primarilly be due to using the whole mile range values from the turn chart, though some of that error can be reduced by interpolating values from the chart.

The cross-track controller only used Eq(56) at each update time to compute a bank angle which would roll the tanker out on course. The 1σ y_m value decreased by a factor of 4. However, there is a slight increase in the error statistics for x_m. That is because when the turn is started, the filter still has about a .4 NM $\hat{y}$ error standard deviation. As a better estimate becomes available during the turn, ϕ_r changes and so, therefore,

Table 1. Rollout Error Statistics

	x_m(NM)			y_m(NM)		
Controller	m	σ	RMS	m	σ	RMS
Open Loop	.83	.71	1.09	.35	1.11	1.16
Cross-Track	.89	1.06	1.38	.14	.23	.27
Closed Loop:						
k=2	.09	.84	.84	.10	.43	.44
k=3	-.21	.54	.58	-.10	.41	.42

does $\dot{\Psi}$. The change in the turn rate from that predicted at the start of the turn, causes the rollout time and hence x_m to vary.

Closed loop control along both axes was simulated next. Results for values of k equal to 2 and 3 are listed. With only a slight increase in the standard deviation of y_m, the statistics for x_m improved considerably. Most of the mean error is eliminated. For k=3, the root mean square error is about half of what it is for the open loop and cross-track controllers. Since the desired values for x_m and y_m are zero, their RMS values, where RMS = $\sqrt{m^2 + \sigma^2}$ are an appropriate, comparative measure of controller performance.

The values for k equal to 2 and 3 were selected from the results of a larger set of runs. In Figure 13, the RMS miss distances are plotted for values of k between 0 and 10. The case of k equal to zero implies cross-track control only: the bank angle which minimized y_m was computed, and no adjustments were made to reduce x_m. As k was increased above zero, the RMS values for x_m decreased, while the y_m RMS values increased slightly. However, for k equal to 9 or more, the bank angle corrections were too great, and the controller produced increasingly large rollout errors. At k equal to 12, the RMS values for x_m and y_m were 9.3 and 3.0 NM respectively. The controller did not seem to be particularly sensitive to changes in gain in the range of k equals 2 to 6. The x miss distances were improved over those of the cross-track controller, and the y miss distances remained small.

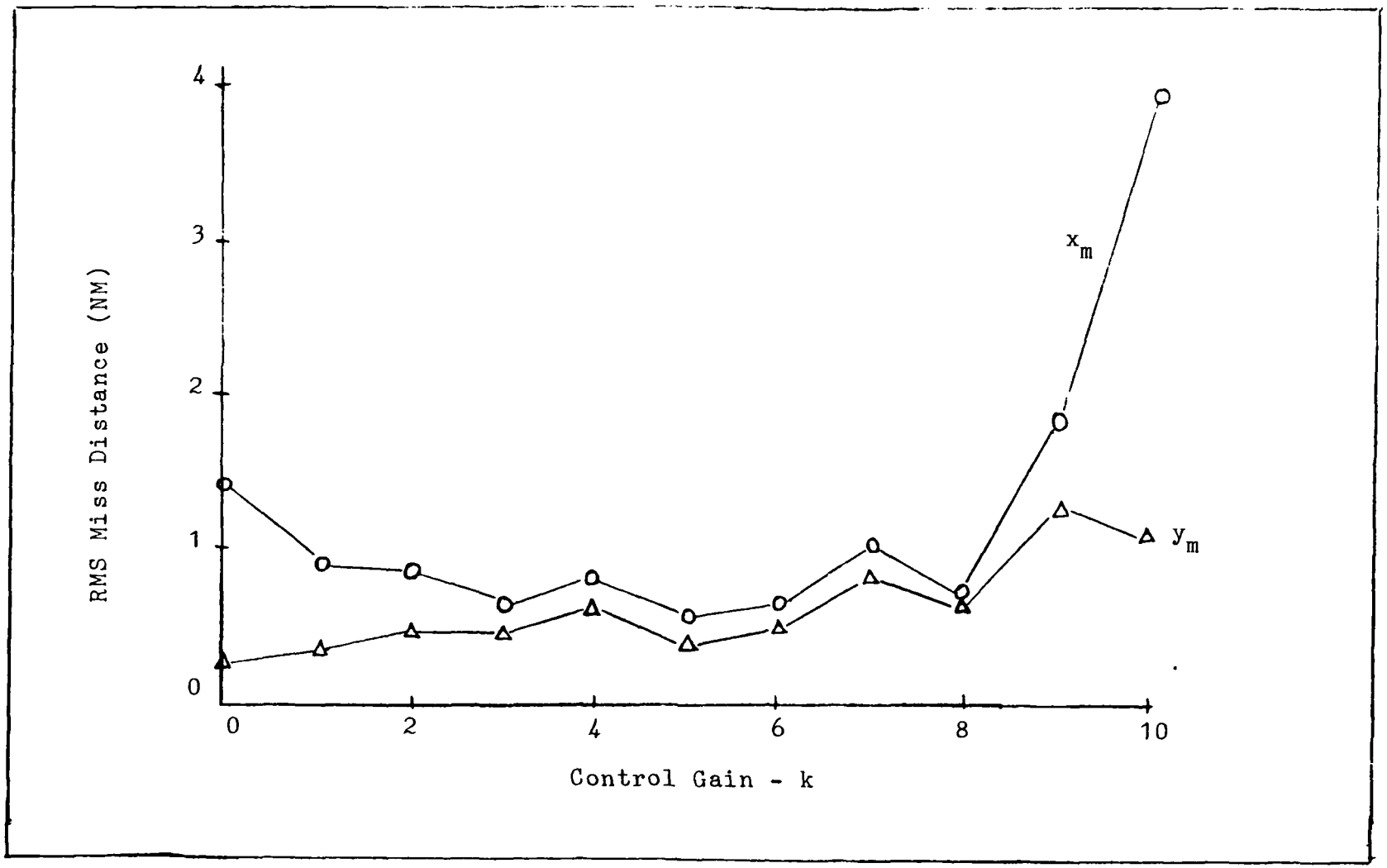

Figure 13. Effect of Control Gain on RMS Miss Distances

A Monte Carlo run was also conducted in which the controller inputs were the true states and not the filter estimates. For a gain of k equal to 3, the resulting x_m RMS value of 0.17 NM and y_m RMS value of 0.09 confirmed that there were no basic flaws in the closed loop control concept itself.

One other case was simulated. A turn from other than nominal conditions was modelled. Such an initial error might be due to pilot error, insufficient time to correct to the desired offset, weather avoidance, and so on. For the open loop, cross-track, and closed loop controllers, the turn was started from an offset 2 NM wider than nominal, and 5 seconds earlier than it should have been.

For this case, the differences in controller performance were more pronounced. The results are listed in Table 2. The open loop controller had large mean errors because it never tried to compensate for the initial deviation. The cross-track controller reduced the y_m RMS value by a factor of 10, but it did not correct

Table 2. Rollout Error Statistics - Turn Initiated From Other Than Nominal Conditions

	x_m(NM)			y_m(NM)		
Controller	m	σ	RMS	m	σ	RMS
Open Loop	.96	.70	1.19	-1.22	1.07	1.62
Cross-Track	.93	1.02	1.38	.04	.13	.14
Closed Loop (k=3)	-.15	.74	.75	-.09	.39	.40

for along-track errors. Finally, the closed loop controller had significantly lower RMS values than the present method for both x_m and y_m. That was because the closed loop corrections reduced the mean rollout errors to near zero.

Even though the filter does not supply a particularly accurate estimate of the receiver's state, the closed loop controller and, to a lesser extent, the cross-track controller, exhibit some advantages over the present open loop method. The cross-track RMS errors are reduced considerably. The closed loop controller also moderately reduces the RMS along-track error. Additionally, these control algorithms compute rendezvous solutions for other than nominal offsets and headings, and can correct for deviations during the turn.

VII Conclusions

The purposes of this research were to develop a digital estimation and control method for conducting air refueling rendezvous, and to evaluate its feasibility and possible benefits. For this study, the design was constrained by present, onboard KC-135 navigation equipment, and the basic geometry of the current method.

A 3 state extended Kalman filter, which only incorporates air-to-air TACAN distance measurements, is not a very accurate estimator, and it appears that a radar estimate would be needed to initialize the filter. However, it does appear to be a simple, stable method of generating a receiver state estimate throughout the final portion of the rendezvous.

Using the filter generated estimate, a single equation control law can significantly reduce cross-track error at rendezvous completion. A control law can also be implemented which decreases the along-track error as well. Using the closed loop control algorithm, the root mean square, cross-track error at rollout was reduced by up to 75% over the present method; and the along-track error was reduced as much as 47%.

The proposed method has two main advantages over the present method. It can compute rendezvous solutions from other than nominal conditions; and it generates a receiver state estimate which enables the tanker to use closed loop control throughout the rendezvous.

The proposed system is entirely compatible with present rendezvous procedures and onboard KC-135 navigation equipment. Incorporating such algorithms in an INS "rendezvous mode" could be a valuable aid for conducting air refueling rendezvous.

VIII Recommendations

The computer simulation results do indicate that the proposed system has some potential advantages over the present method. The next step should be a more complete analysis of the models and designs developed here. Several areas for further study immediately come to mind.

The truth model could be improved with a stochastic model for the tanker's dynamics as well as the receiver's. Such a model would be better for evaluating different controller designs because the effect of deviations during the turn could be evaluated. In this study, only initial deviations were simulated. Such a model could also provide a basis for a stochastic control design analysis.

There are several estimation issues yet to be considered. A sensitivity analysis of the filter to modelling errors should be done, and different aircraft types and airspeeds should be simulated. The effect of the rendezvous geometry on observability could also be investigated.

A present hardware constraint was imposed for this study. However, given the limited filter accuracy achieved, the potential advantages of incorporating other equipment might be considered. For example, the AN/ARN 139 (V) TACAN system which provides air-to-air bearing as well as distance information could be considered (Ref 17).

The potential advantages of closed loop control were investigated, but only one algorithm was developed. Other ad hoc methods could be investigated as well as stochastic control methods.

A vital area which was barely considered in this study is the onboard computer. The estimation and control algorithms need to be evaluated partly on the basis of computation time, memory requirements, and so on. Also, the algorithms developed here might be simplified further.

Very little work has been done in the past on the air refueling rendezvous problem. Therefore, research in just about any area of the problem might result in significant improvements.

References

1. Delco Electronics Division. Technical Description, Carousel IV-E Inertial Navigation System. S77-53. General Motors Corporation, Santa Barbara, California, June 1977.

2. Widnall, William S. and Grundy, Peter A. Inertial Navigation System Error Models. Intermetrics Incorporated, Cambridge, Massachusetts, May 1973. (AD 912 489L).

3. 443d Technical Training Squadron. Academic Student Guide, C-141 Pilot Air Refueling Qualification Course. Document no. 4P6-20. Altus Air Force Base, Oklahoma, August 1980.

4. Bobick, J.C. and Bryson, A.E.,Jr. "Improved Navigation by Combining VOR/DME Information and Air Data," AIAA Paper No. 71-928, AIAA Guidance, Control, and Flight Mechanics Conference, Hempstead, New York, August 1971.

5. Maybeck, Peter S. Stochastic Models, Estimation, and Control, Volume 1. Academic Press, New York, 1979.

6. Winter, H. "Experiences in Flight Testing Hybrid Navigation Systems," AGARD Lectures Serie No. 82, Practical Aspects of Kalman Filtering Implementation, May 1976. (AD-A024 377).

7. AFM 51-37. Instrument Flying. Department of the Air Force, Washington, D.C., December 1976.

8. Maybeck, Peter S. Filter Design for a TACAN-Aided Baro-Inertial System with ILS Smoothing Capability. AFFDL-TM-74-52, Air Force Flight Dynamics Laboratory, Wright-Patterson Air Force Base, Ohio.

9. Sherard,G.W. "Range Noise Analysis of the ARN-118 TACAN," Internal letter, Rockwell International, Collins Groups, Cedar Rapids, Iowa, 11 March 1981.

10. Collins Government Avionics Division. Collins TCN-118 (AN/ARN-118(V)) Airborne TACAN System. Description 523-0765893. Rockwell International, Cedar Rapids, Iowa, 1 April 1979.

11. Luciani, Vincent J. Accuracy Test of an Air-to-Air Ranging and Bearing System. Report No. FAA-RD-77-59, June 1977. (AD A043392).

12. Maybeck, Peter S. Stochastic Models, Estimation, and Control, Volume 2. Academic Press, New York, 1982.

13. Wauer, John C. "Practical Considerations in Implementing Kalman Filters," AGARD Lecture Series No. 82, Practical Aspects of Kalman Filtering Implementation, May 1976. (AD-A024 377).

14. Musick, S.H. SOFE: A Generalized Digital Simulation for Optimal Filter Evaluations, User's Manual. AFWAL-TR-80-1108, Air Force Wright Aeronautical Laboratories, Wright-Patterson Air Force Base, Ohio, October 1980.

15. Musick, S.H. SOFEPL: A Plotting Postprocessor for 'SOFE', User's Manual. AFWAL-TR-80-1109, Air Force Wright Aeronautical Laboratories, Wright-Patterson Air Force Base, Ohio, November 1981.

16. T.O. 1-1C-1-3. KC-135 Flight Crew Air Refueling Procedures. Department of the Air Force, Washington, D.C., 1 November 1980.

17. Collins Government Avionics Division. Collins AN/ARN-139(V) Airborne TACAN. Technical Data Sheet. Rockwell International, Cedar Rapids, Iowa, 25 February 1981.

VITA

Captain James T. Rivard was born in Detroit on November 30, 1952. In 1970, he graduated from Divine Child High School in Dearborn, Michigan and entered the United States Air Force Academy. There, he was awarded the degree of Bachelor of Science in Astronautical Engineering in 1974. After pilot training at Williams Air Force Base, Arizona, Captain Rivard was assigned to the 30th Military Airlift Squadron, McGuire Air Force Base, New Jersey. For five years, he flew as a C-141 pilot, aircraft commander, and instructor pilot until he entered the Air Force Institute of Technology in 1981.

Permanent address: 2216 Drexel
Dearborn, Michigan 48128

UNCLASSIFIED

SECURITY CLASSIFICATION OF THIS PAGE *(When Data Entered)*

REPORT DOCUMENTATION PAGE		READ INSTRUCTIONS BEFORE COMPLETING FORM
1. REPORT NUMBER AFIT/GA/EE/82D-1	2. GOVT ACCESSION NO. AD-A126 543	3. RECIPIENT'S CATALOG NUMBER
4. TITLE *(and Subtitle)* DIGITAL ESTIMATION AND CONTROL FOR AIR REFUELING RENDEZVOUS		5. TYPE OF REPORT & PERIOD COVERED MS Thesis 6. PERFORMING ORG. REPORT NUMBER
7. AUTHOR(s) James T. Rivard Capt		8. CONTRACT OR GRANT NUMBER(s)
9. PERFORMING ORGANIZATION NAME AND ADDRESS Air Force Institute of Technology (AFIT-EN) Wright-Patterson AFB, Ohio 45433		10. PROGRAM ELEMENT, PROJECT, TASK AREA & WORK UNIT NUMBERS
11. CONTROLLING OFFICE NAME AND ADDRESS		12. REPORT DATE December 1982 13. NUMBER OF PAGES 94
14. MONITORING AGENCY NAME & ADDRESS*(if different from Controlling Office)*		15. SECURITY CLASS. *(of this report)* Unclassified 15a. DECLASSIFICATION DOWNGRADING SCHEDULE

16 DISTRIBUTION STATEMENT *(of this Report)*

Approved for public release; distribution unlimited

17. DISTRIBUTION STATEMENT *(of the abstract entered in Block 20, if different from Report)*

18. SUPPLEMENTARY NOTES

Approved for public release: IAW AFR 190-17.

LYNN E. WOLAVER
Dean for Research and Professional Development
Air Force Institute of Technology (AIC)
Wright-Patterson AFB OH 45433

4 JAN 198

19. KEY WORDS *(Continue on reverse side if necessary and identify by block number)*

Estimation
Control
Air Refueling
Rendezvous
TACAN
Kalman Filter
Model

20. ABSTRACT *(Continue on reverse side if necessary and identify by block number)*

Estimation and control algorithms were developed for use by a tanker aircraft conducting an air refueling rendezvous. A stochostic model of a typical rendezvous was developed first. Then an extended Kalman filter which uses air-to-air TACAN distance measurements was designed. Also, algorithms were derived for computing the tanker's appropriate offset, turn point, and closed loop bank angle commands during the final turn of a

DD FORM 1 JAN 73 1473 EDITION OF 1 NOV 65 IS OBSOLETE

UNCLASSIFIED

SECURITY CLASSIFICATION OF THIS PAGE *(When Data Entered)*

point-parallel rendezvous.

In Monte Carlo simulations, a 3 state extended Kalman filter provided a stable, though limited, means of estimating the receiver's position and velocity throughout the rendezvous. Also, the control algorithms exhibited two advantages over the present rendezvous method: turn point solutions could be computed for other than nominal offsets and headings, and bank angle commands during the turn reduced position errors at rendezvous completion. When compared to the present method, root mean square, cross-track distance errors at rollout were reduced as much as 75%, and along-track errors were reduced up to 47%.

END

FILMED

3-83

DTIC